Exceptionally Long ($\geq$2.9 Å) CC Bonding Interactions in π-$[TCNE]_2^{2-}$ Dimers: Two-Electron Four-Center Cation-Mediated CC Bonding Interactions Involving π* Electrons

Rico E. Del Sesto,[a] Joel S. Miller,*[a] Pilar Lafuente,[b] and Juan J. Novoa*[b]

Dedicated to Professor Owen W. Webster for his pioneering discoveries in the area of TCNE chemistry and Professor Jean-Marie Lehn for his pioneering discoveries in supramolecular chemistry

Abstract: Three groups of singlet ground state $[TCNE]_2^{2-}$ (TCNE = tetracyanoethylene) dimers with characteristic intradimer CC separations (r) and dihedral angles (d) [i.e., group S_t ($r \sim 1.6$ Å; $d = 180°$), L_t ($r \sim 3.5$ Å; $d = 180°$), and L_c ($r \sim 2.9$ Å; $d = \sim 0°$); notation: S/L: short/long bond length; subscript t/c: *trans*/*cis*, respectively] are experimentally characterized. The S_t group is comprised of σ-dimers of $[TCNE]^{\bullet-}$ and octacyanobutanediide, $[C_4(CN)_8]^{2-}$, which have a typical, albeit long, sp^3-sp^3 σ bond ($r \sim 1.6$ Å) between each $[TCNE]^{\bullet-}$ moiety and characteristic ν_{CN}, ν_{CC}, and δ_{CCN} IR absorptions. The L groups are structurally characterized as π-dimers of $[TCNE]^{\bullet-}$ that are either eclipsed with $r \sim 2.9$ Å (L_c) and the nitriles bend away from the nominal TCNE plane away from the center of the dimer by 5.0° ($\sim sp^{2.17}$) or are noneclipsed with $r \sim 3.5$ Å (L_t) and the nitriles bend toward the center of the dimer by 1.9° ($\sim sp^{2.06}$). Ab initio computations on isolated dimers were used to study the formation and stability of these exceptionally long CC ($\geq$2.9 Å) bonding interactions as well as the process of π-$[TCNE]_2^{2-}$ dimer formation for the L_c and L_t groups. The results of these computational studies show that the ground-state potential curve is that of a closed-shell/open-shell singlet, depending on the distance. The short S_t group ($r \sim 1.6$ Å) of dimers in this surface are true minimum-energy structures; however, the L_t and L_c groups are unstable, although two different nonphysical minima are found when imposing a double occupancy of the orbitals. These minima are metastable relative to dissociation into the isolated $[TCNE]^{\bullet-}$ units. Consequently, the existence of dimer dianions in crystals is due to cation$\cdots$$[TCNE]^-$ interactions, which provide the electrostatic stabilization necessary to overcome the intradimer electrostatic repulsion. This cation-mediated $\pi^*-\pi^*$ $[TCNE]^-\cdots[TCNE]^-$ interaction complies with Pauling's definition of a chemical bond. This bonding interaction involves the π* orbitals of each fragment, and arise from the overlap of the b_{2g} SOMO on each of the two $[TCNE]^{\bullet-}$s to form a filled b_{2u} $[TCNE]_2^{2-}$ orbital. Although a π dimer typically forms, if the fragments are close enough a σ dimer can form. Due to the presence of cation-mediated intradimer CC bonding interactions the L_c group of π-$[TCNE]_2^{2-}$ dimers exhibits experimentally observable ν_{CN} IR absorptions at 2191 ± 2 (m), 2173 ± 3 (s), and 2162 ± 3 cm^{-1} (s) and ν_{CC} at 1364 ± 3 cm^{-1} (s) as well as a new UV-Vis feature in the range of 15000 to 18200 cm^{-1} (549 to 667 nm) and averaging 16825 ± 1180 cm^{-1} (594 nm) assigned to the predicted new intradimer $^1A_{1g} \rightarrow {}^1B_{1u}$ transition and is purple on reflected light. Upon cooling to 77 K in 2-methyl tetrahydrofuran, this new band occurs at 18940 cm^{-1} (528 nm) for $\{[Et_4N]^+\}_2[TCNE]_2^{2-}$, and the yellow solution turns deep red. Group L_t is characterized by ν_{CN} absorptions at 2215 ± 2, 2197 ± 3, and 2180 ± 4 cm^{-1} and ν_{CC} at 1209 ± 9 cm^{-1} (w), while group S_T has ν_{CN} bands at 2215 ± 4, 2157 ± 3, and 2107 ± 4 cm^{-1} and ν_{CC} at 1385 ± 1 cm^{-1} (vs).

Keywords: ab initio calculations · bonding interactions · dimerization · electronic structure · supramolecular interactions · TCNE

[a] Prof. J. S. Miller, Dr. R. E. Del Sesto
Department of Chemistry
University of Utah
315 S. 1400 E. RM 2124
Salt Lake City, UT 84112-0850 (USA)
Fax: (+1) 801-581-8433
E-mail: jsmiller@chemistry.utah.edu

[b] Prof. J. J. Novoa, P. Lafuente
Department of Physical Chemistry
University of Barcelona
Av. Diagonal, 647, E-08028, Barcelona (Spain)
E-mail: novoa@qf.ub.es

Supporting information for this article [shape of the HOMO and SOMO orbitals, $\Delta(r)$ for the S_t conformation, and plot of $\nu_{max}(r)$] is available on the WWW under http://www.chemeurj.org/ or from the author.

0947-6539/02/0821-4894 $ 20.00+.50/0 *Chem. Eur. J.* **2002**, *8*, No. 21

Introduction

Strong organic electron acceptors (A), for example, tetracyanoethylene (TCNE), 7,7,8,8-tetracyano-*p*-quinodimethane (TCNQ), perfluoro-7,7,8,8-tetracyano-*p*-quinodimethane ($TCNQF_4$), 2,3-dichloro-5,6-dicyanobenzoquinone (DDQ), and hexacyanobutadiene, form stable electron transfer salts that contain $[A]^{\bullet-}$. Studies of these salts have been essential for the discovery and development of molecule-based metals[1] (e.g., [TTF][TCNQ]; TTF = tetrathiafulvalene), which subsequently lead to the discovery of molecule-based superconductors[2] and magnets[3] (e.g., $[Fe(C_5Me_5)_2][TCNE]$). These strong acceptors have the common features of being planar, having two reversible one-electron reductions, Table 1, and the radical anions and diamagnetic dianions are stable species.[4]

Table 1. Reversible one-electron reduction potentials[a] for representative strong acceptors.

Acceptor	$E^{\circ/-}$ [V]	$E^{-/2-}$ [V]
TCNE	0.15	−0.57[b]
TCNQ	0.17	−0.37[b]
$TCNQF_4$	0.53	0.02[b]
DDQ	0.59	−0.25[9]
$C_4(CN)_6$	0.60	0.02[9]
cyanil	0.90	0.09[b]
$C_3[C(CN)_2]_3$	1.13[c]	0.34[b]

[a] Versus SCE in MeCN (Pt electrode; 0.1 M $[nBu_4N][ClO_4]$). [b] M. D. Ward, *Electroanal. Chem.* **1989**, *16*, 182. [c] The neutral form of the acceptor has not been isolated.

The structures of diamagnetic A° and $[A]^{2-}$ form few conformers, while $[A]^{\bullet-}$ may form a myriad of structures. The anion of TCNE has been structurally isolated as $[TCNE]^{\bullet-}$ (**1**),[5] its σ-dimer octacyanobutanediide, $[C_4(CN)_8]^{2-}$ (**2**),[6] and its π-dimer π-$[TCNE]_2^{2-}$ (**3**).[7, 8] Whereas **1** and **3** need not be

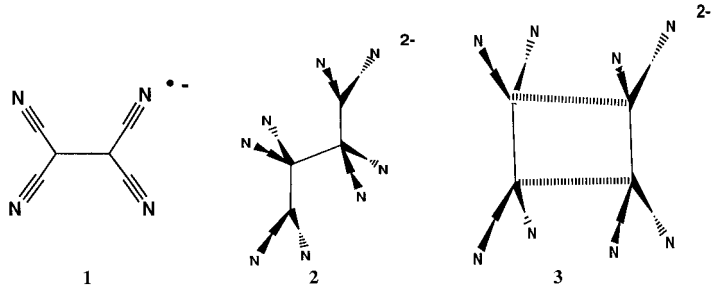

1 2 3

N-metal coordinated, dimer **2** has only been isolated as being μ_4-*N*-metal coordinated. $[TCNQ]^{\bullet-}$ exhibits the same structural diversity as $[TCNE]^{\bullet-}$; however, it additionally forms π-mers that include extended, uniform one-dimensional chains which form the basis of many molecule-based metals.[1] While $[TCNE]^{\bullet-}$ and $[TCNQ]^{\bullet-}$ are more extreme in their structural variation, other $[A]^{\bullet-}$s have been characterized to form the π-$[A]_2^{2-}$ structure, sometimes exclusively as noted for cyanil.[9]

Structure **3**, as well as other π-$[A]_2^{2-}$ dimers, represents an unusual class of organic compounds that possess exceptionally long CC bonding interactions, that is, 2.827[7i] to 3.51 Å[7f] (Table 2). These CC distances are twice that of the typical sp^3-sp^3 CC bond (1.54 Å), and are also substantially longer than elongated CC bonds that have been reported to be as long as 1.73 Å.[10] Thus, these dimers have intermolecular π–π bonding interactions, normally taken as a subclass of van der Waals interactions, as the distances are significantly shorter that the sum of the van der Waals radii of the two atoms involved in the shortest contact distances. Furthermore, each structure for A = TCNE (**1**–**3**) has characteristic ν_{CN} IR absorptions (Table 2), namely, **1**: two-line pattern; **2** and **3**: three-line patterns that span $\geq 100\ cm^{-1}$ for **2**, and $\sim 30\ cm^{-1}$ for **3**. π-$[TCNE]_2^{2-}$ dimers were selected with respect to π-$[TCNQ]_2^{2-}$ and other π-$[A]_2^{2-}$ dimers for detailed study owing to their relative simplicity and fewer observed structures.

The first structurally characterized $[TCNE]_2^{2-}$ dimer, $[Fe(C_5H_4)_2C_3H_6]_2[TCNE]_2$, was reported in 1981,[7c] while spectroscopic evidence for complex or dimer formation existed in the literature as early as 1960.[11, 12] Herein, we target the understanding of the unusual intradimer bonding associated with π-$[TCNE]_2^{2-}$, and in particular the exceptionally long CC bonding interactions (≥2.9 Å) observed for some TCNE electron-transfer salts. Furthermore, the principles that govern the dimerization process of $[TCNE]^{\bullet-}$ are analyzed, as it is the prototype for the bonding in related π dimers observed for other strong electron acceptors. After a detailed analysis of the geometries of these dimers, a complete analysis of the electronic structures of these compounds was performed and compared to observation in order to understand the spectroscopic features of these dimers. We also focus on the energetics of the dimer formation process, and a search of the number of minimum-energy structures present in their potential-energy surface was performed, as well as investigations into the relative stability of the singlet and triplet states. Finally, we will present experimental spectroscopic (UV-visible and IR spectra) evidence validating this theoretical study.

Results and Discussion

$[TCNE]_2^{2-}$ dimer geometry: The known structures of TCNE anions (**1**–**3**; Table 2) can be represented by structure **4** with *r* being the intradimer C_1-C_3 distance, and *d* being the dihedral angle between each $[TCNE]^{\bullet-}$ moiety, that is, C_2-C_1-C_3-C_4. A

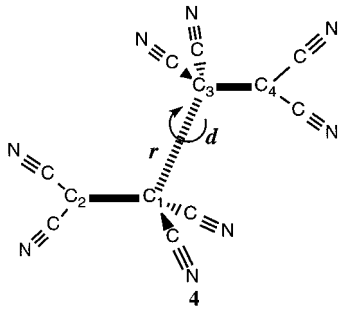

4

plot of the experimentally known values of $d(r)$ (Figure 1) reveals three disjoint groups (S_t, L_t, and L_c; notation: S/L: short/long bond length; subscript t/c: *trans*/*cis*, respectively). The S_t group is comprised of dimers with $r < 1.7$ Å and the two

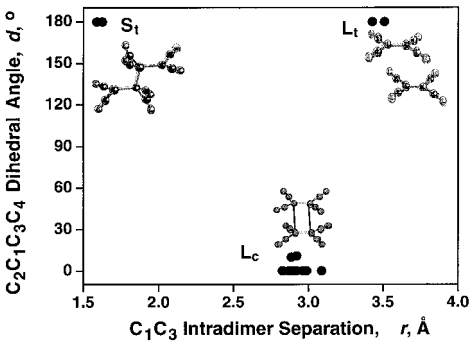

Figure 1. Plot of $d(r)$ for the structurally characterized $[TCNE]_2^{2-}$ dimers (see Table 2).

$[TCNE]^-$ units *trans* to each other ($d \sim 180°$). The L_c and L_t groups have $r > 2.8$ Å, but for the L_c group the two $[TCNE]^-$ units are *cis* ($d \sim 0°$), while in the L_t group they are *trans* ($d \sim 180°$). Table 2 also lists the intradimer CC distance, the deviation from the planarity of each nitrile, and the ν_{CN} IR stretching frequencies for these dimers.

$M^{II}(NCMe)_2[C_4(CN)_8]$ (M = Mn, Fe) are examples of an S_t dimer and possess μ_4-*N*-$[C_4(CN)_8]^{2-}$ (**2**) with $r \sim 1.6$ Å; the central C atoms exhibit clear sp^3 hybridization.[6] Hence, the $[TCNE]^-$ fragments are connected by a typical, albeit long[10] σ-bond, and the dimer is the octacyanobutanediide dianion, $[C_4(CN)_8]^{2-}$ (**2**).[6] Similar σ-$[TCNQ]_2^{2-}$ dimers have also been reported.[13] In contrast, the L_c and L_t dimers with $r > 2.8$ Å are best described by two parallel nearly planar $[TCNE]^-$; the central C atoms are $\sim sp^2$ hybridized rather than $\sim sp^3$ hybridized. These are π dimers of type **3** because the intradimer CC bonding primarily occurs through the σ-like overlap of p orbitals on adjacent $[TCNE]^-$'s (**5a**), in sharp contrast to conventional π bonding (**5b**) as observed for alkenes and alkynes, which involves a lateral overlap of the p orbitals.

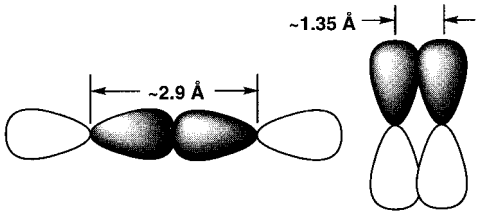

5a **5b**

Nature of the $[TCNE]_2^{2-}$ intradimer interactions: The properties of the $[A]_2^{2-}$ dimers are determined by the anionic nature of the monomers and the existence of an unpaired electron on each of the monomers. Consequently, as shown in Figure 2, two major factors dominate the interaction energy (E_{int}) between the monoanionic monomers: 1) the electrostatic

Table 2. Intradimer CC distances, deviation from planarity, ν_{CN}, ν_{C-CN}, and ν_{CC} frequencies for structurally characterized S_t, L_c, and L_t groups of

Compound	Group	d [°]	Form	r [Å]	C–C [Å]	Deviation from plane [°][a]	ν_{CN} [cm^{-1}]	
$Fe^{II}[C_4(CN)_8](NCMe)_2 \cdot MeCN$[6]	S_t	179.91	μ_4-π-$[C_4(CN)_8]_2^{2-}$	1.627	1.627		2213 (w)	2153 (s)
$Mn^{II}[C_4(CN)_8](NCMe)_2 \cdot CH_2Cl_2$[6]	S_t	179.96	μ_4-π-$[C_4(CN)_8]_2^{2-}$	1.59	1.59		2212 (w)	2159 (s)
$Co^{II}[C_4(CN)_8](NCMe)_2 \cdot CH_2Cl_2$	S_t		μ_4-π-$[C_4(CN)_8]_2^{2-}$	[c]	[c]		2223 (m)	2159 (s)
Average values	S_t	179.94	μ_4-π-$[C_4(CN)_8]_2^{2-}$	1.61	1.61		2215 (w)	2157 (s)
Standard deviation		±0.02		±0.01	±0.01		±4	±3
$[Cu(PPh_3)_3(TCNE)]_2$[7a]	L_c	0.136	π-σ-$TCNE]_2^{2-}$	2.92	1.397	4.9	2193	2173
$[Cr(C_6H_6)_2]_2[TCNE]_2$[7b]	L_c	0.045	π-$[TCNE]_2^{2-}$	2.904	1.436	6.2	2189	2170
$[Cr(C_6Me_3H_3)_2]_2[TCNE]_2$[7b]	L_c	0.084	π-$[TCNE]_2^{2-}$	3.09[b,d]	1.45[b,c]	[c]	[c]	[c]
$[Fe(C_5H_4)_2C_3H_6]_2[TCNE]_2$[7c,b]	L_c	0.030	π-$[TCNE]_2^{2-}$	2.90	1.35	5	2191	2169
$Na_2[TCNE]_2(glyme)_2$[7j]	L_c	0.000	μ_4-π-$[TCNE]_2^{2-}$	2.961	1.423	2.3	[c]	[c]
$K_2[TCNE]_2(glyme)_2$[7d]	L_c	0.062	μ_4-π-$[TCNE]_2^{2-}$	2.987	1.420	3.6	[c]	[c]
$Cs_2[TCNE]_2$[7l]	L_c	10.000	μ_{15}-π-$[TCNE]_2^{2-}$	2.89	1.43	5.4	2197	2179
$[Fe(C_5H_5)(C_5Me_5)]_2[TCNE]_3(THF)$[7e]	L_c	0.061	π-$[TCNE]_2^{2-}$	2.903	1.372	5.8	2190	2173
$[Fe(C_5H_5)(C_5Me_5)]_2[TCNE]_3(CH_2Cl_2)$[7e]	L_c	0.047	π-$[TCNE]_2^{2-}$	2.833	1.459	6.4	2190	2174
$[Et_4N]_2[TCNE]_2$[7i]	L_c	0.000	π-$[TCNE]_2^{2-}$	2.827	1.418	6.6	2191	2170
$[iPr_4N]_2[TCNE]_2$[7i]	L_c	0.049	π-$[TCNE]_2^{2-}$	2.870	1.408	5.2	2191	2175
$[(Me_2N)_2CC(NMe_2)_2][TCNE]_2$[7g,h]	L_c	10.94	π-$[TCNE]_2^{2-}$	2.922	1.400	4.0	2193	2173
$Tl_2[TCNE]_2$[7g]	L_c	0.087	μ_{16}-π-$[TCNE]_2^{2-}$	2.874	1.51	4.4	2190	2173
[HAOC][TCNE]$_2$[7k],[k]	L_c		π-$[TCNE]_2^{2-}$	[c]	[c]	[c]	2190	2174
Average values	L_c	1.65	π-$[TCNE]_2^{2-}$	2.90	1.405	5.0	2191	2173
Standard deviation		±4.1		±0.05	±0.03	±1.3	±2	±3
α-[TTF][TCNE][7f]	L_t	178.81	π-$[TCNE]_2^{2-}$	3.426[d,e]	1.40	−2.8 [g]	2218 (m)	2200 (s)
β-[TTF][TCNE][7f]	L_t	178.93	π-$[TCNE]_2^{2-}$	3.508[d,f]	1.397	−1.0[g]	2214 (m)	2198 (s)
Average values	L_t	179.87	π-$[TCNE]_2^{2-}$	3.47	1.399	−1.9[g]	2216[h]	2197[h]
Standard deviation		±0.06		±0.04	±0.002	±0.9	±2	±3

[a] The average NC-C-C···C dihedral angle minus 90° from CrystalMaker5. [b] Disordered—excluded from average. [c] Not reported. [d] Noneclipsed. [e] Shortest intradimer CC distance = 3.48 Å. [f] Shortest intradimer CC distance = 3.52 Å. [g] Negative value indicates bending toward the center of the dimer. [h] The previously reported values of 2215, 2194, 2178 cm^{-1} are included in the average:[7g] M. Meneghetti, C. Pecile, *J. Chem. Phys.* **1996**, *105*, 397. [i] Spectrum not observed due to formation of $M[TCNE]_2$ under the conditions of the experiment. [j] Not assignable absorptions from the cation in this region. [k] Hexaazaoctadecahydrocoronene. [l] Some or all of the spectroscopic data—this work.

0947-6539/02/0821-4896 $ 20.00+.50/0 *Chem. Eur. J.* **2002**, *8*, No. 21

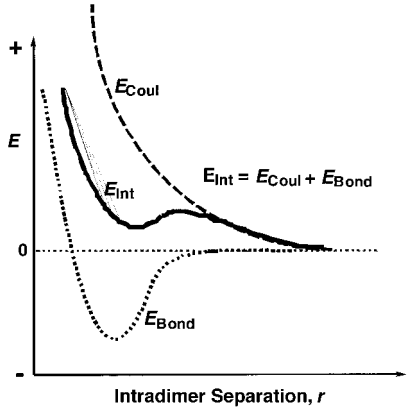

Figure 2. Diagram showing how the total interaction energy curve (E_{int}) is built by addition of the Coulombic (E_{coul}) and bonding (E_{bond}) components.

coulombic repulsion (E_{coul}) present between the two anionic $[A]^{\bullet-}$ fragments and 2) the attractive forces generated by the unpaired electrons (E_{bond}), which try to form either an intradimer σ or π bond. The total interaction is $E_{int} = E_{coul} + E_{bond}$. If E_{coul} dominates (i.e., $E_{coul} > E_{bond}$), the two $[A]^{\bullet-}$ units will repel each other at all distances, and there will be no minimum-energy structures on their potential-energy surface. If, however, $E_{bond} > E_{coul}$ there will be a stable energy minimum on the surface (see Figure 2). Additionally, when $E_{bond} \sim E_{coul}$ metastable dimers form, that is, the energy of such minimum lies above the energy of two $[A]^{\bullet-}$ monomers, but the dimer does not break into these fragments due to the presence of a barrier towards dissociation (Figure 2). If E_{coul} becomes weaker or the bonding interactions between the two $[A]^{\bullet-}$ monomers becomes stronger, the metastable dimer increases its stability and the barrier is reduced. At some point, the dimer goes from being metastable to being stable and the barrier disappears (Figure 2). Metastable species cannot form in the gas phase at finite temperature as the thermal energy is less than the barrier for the formation of the dimer from its fragments. Nevertheless, it can occur in a crystal if the electrostatic cation–$[A]^-$ interaction is strong enough to overcome the repulsive coulombic energy barrier associated with the $[A]^{\bullet-}$–$[A]^{\bullet-}$ interaction. Although the existence of $[A]_2^{2-}$ dimers, as represented by $[TCNE]_2^{2-}$, in the solid suggests that a stable or metastable dimer is formed,[6–8] a detailed characterization requires a computation of the energetics of these dimers in the regions of the experimental geometry, both isolated and in the crystal environment. It can also occur in solution if the solvent–anion interactions overcome the anion–anion coulombic repulsion.

Ab initio UBLYP/6-31+G(2d,2p) computations on an isolated $[TCNE]^{\bullet-}$ fragment shows that it has a planar structure similar to that obtained for $TCNE^{\circ}$,[14, 15] by using the same geometry and method, except that the central CC distance, increases from 1.358 Å in $TCNE^{\circ}$ to 1.392 Å in the $[TCNE]^{\bullet-}$, while the C≡N distance undergoes a minor increase from 1.158 to 1.167 Å. The extra electron of the anion is located in the $TCNE^{\circ}$ b_{2g} SOMO of π symmetry (Figure S1 in the Supporting Information). This orbital primarily resides on the central C and N atoms, with similar weights for each of those atoms. The Mulliken population analysis for $[TCNE]^{\bullet-}$ (Table 3) indicates that the central C and the N atoms equally share the extra electron, each with 0.18 e^- (a value obtained by subtracting the atomic charges of $[TCNE]^{\bullet-}$ and $TCNE^{\circ}$ monomers displayed in Table 3). This agrees with the experimental data from single-crystal polarized neutron diffraction studies.[5c] The tendency to delocalize the charge on the peripheral atoms cannot be attributed solely to the electronegativity of the CN group, as it is neither found for $[C_2H_4]^{\bullet-}$[16a] nor $[C_2F_4]^{\bullet-}$,[16b] although F is more electronegative than CN. Therefore, such behavior can only be associated with delocalization due to the presence of low-energy resonance forms in which the unpaired electron is delocalized over the CN groups (**6**).

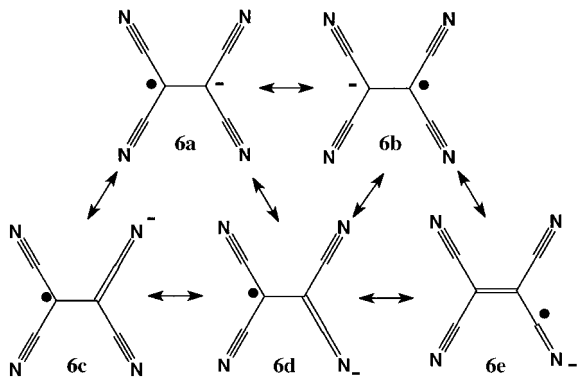

π-$[TCNE]_2^{2-}$ dimers.

ν_{CN} [cm^{-1}]	ν_{CC} [cm^{-1}]	δ_{C-CN} [cm^{-1}]			ν_{max} [cm^{-1}]
2109 (w)	1203 (w)	558	537	509 [l]	[i]
2100 (w)	1219 (w)	556	530	504 [l]	[i]
2112 (w)	1204 (w)	556	539	510	[i]
2107 (w)	1209 (w)	557	535	508	[i]
±4	±9	±1	±5	±3	
2162	1365	[j]	[j]	[j]	17100
2159	1365	553	528	514	17200
[c]	[c]	[c]	[c]	[c]	[c]
2161	1366	548	526	513	15000
[c]	[c]	[c]	[c]	[c]	[c]
[c]	[c]	[c]	[c]	[c]	[c]
2169	1355	551	539	521	17900
2159	1365	547		514	[c]
2160	1364	549	530	517	[c]
2163	1365	545	526	516	16850
2161	1365	551	528	513	18300
2163	1365	547	528	515	17250
2162	1361	550	534	518	15100
2159	1363	[j]	528	513	[c]
2162	1364	549	530	516	16840
±3	±3	±2	±4	±3	±1200
2186 (m), 2177 (w)	1385 (vs)	593, 581	536	520	[c]
2179 (s)	1385 (vs)	585	534	520	[c]
2180[h]	1385	586	535	520	[c]
±4	±1	±3	±1	±1	

Table 3. Net atomic charges obtained after a Mulliken population analysis of the B3LYP/6–31 + G(2d,2p) wavefunction on the atoms of the neutral and monoanionic $[C_2X_4]^n$ monomers (X = H, F, CN; $n = 0, -1$).

Molecule	Atom	Charge	
		$n = 0$	$n = -1$
C_2H_4	C	−0.237	−0.737
	H	0.119	0.119
C_2F_4	C	0.590	−0.217
	F	−0.295	−0.141
$C_2(CN)_4$, (TCNE)	C (*C*CN)	0.996	0.820
	C (*C*N)	−0.294	−0.272
	N (C*N*)	−0.203	−0.387

When the SOMO of one $[TCNE]^{\bullet-}$ fragment interacts with that of the other fragment in the L_c conformation, they combine to form a bonding and antibonding orbital of b_{2u} and b_{1g} symmetry, respectively (Figure 3). If the energy separation

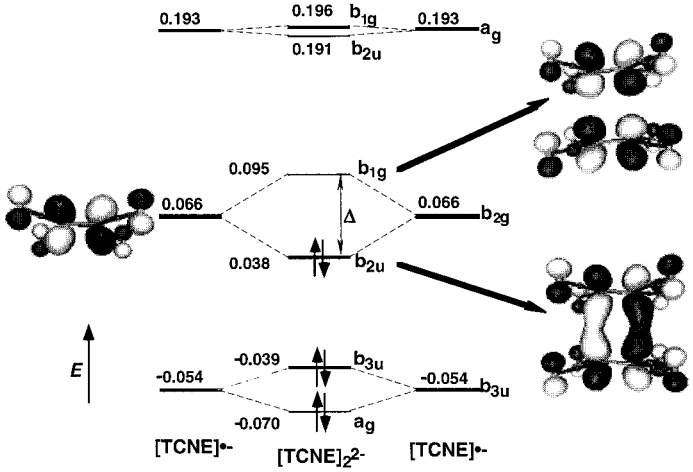

Figure 3. Shape of the $[TCNE]^{\bullet}$ dimer orbitals generated from the HOMO, SOMO, and LUMO orbitals of the $[TCNE]^{\bullet-}$ fragments. The calculated energies are in atomic units (au; 1 au = 627.51 kcal mol^{-1} = 27.21 eV = 219 292 cm^{-1}).

(Δ) between these two orbitals is small, as occurs at large values of *r*, each orbital will be singly occupied and the $b_{2u}^1b_{1g}^1$ configuration is expected to be the lowest in energy, similar to what occurs when two H atoms interact to form H_2.[17] This configuration gives rise to an open shell singlet (S_1) or a triplet (T_o) state, both giving rise to two equivalent $[TCNE]^-$ fragments at dissociation. As shown in Figure 4, the energy of these two states increases as *r* decreases. Consequently, no new bonds are formed between the fragments in any of these two states.

As *r* decreases, Δ increases and the $b_{2u}^2b_{1g}^\circ$ configuration, which at dissociation lies high above the $b_{2u}^1b_{1g}^1$ configuration because it gives rise to dissociation into $[TCNE]^\circ$ and $[TCNE]^{2-}$ fragments, becomes the most stable. This is again similar to the situation found when two H atoms interact to form H_2.[17] This configuration is associated with the lowest energy state (S_o) and E_{bond} dominates E_{int} at short distances, thus giving rise to the formation of a bonding interaction between the fragments in the absence of an E_{coul} term.

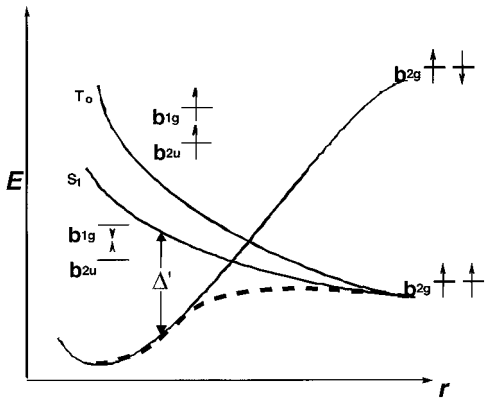

Figure 4. Shape of the diabatic energy curves for the lowest closed-shell singlet, open-shell singlet, and triplet states of a doublet radical. The broken line is the adiabatic obtained by allowing the S_o and S_1 diabatic curves to interact.

This bonding interaction is unique in three aspects: 1) it involves 2e$^-$ residing over four chemically equivalent carbon atoms; 2) it involves the π* orbitals of each fragment (**5a**); and (3) it is supramolecular, as is induced by the electrostatically attractive cation ··· anion interactions, which enables the electrostatically repulsive anions to be sufficiently close to each other such that their SOMOs can overlap. As its existence is associated with the overlap of the π* orbitals of each fragment, the bonding interaction will be found whenever two $[TCNE]^-$ fragments are placed at such a short distance from each other, either because the interaction between these two fragments is energetically stabilizing, or because some external force drives them together. Multicentered two-electron (including four-centered) bonding[18] has been reported for several boranes,[19] and for the structurally constrained, but not structurally characterized 1,3-dehydro-5,7-adamantanediyl[20a] and pagodane dications;[20b] however, this is the first example for a carbon-based system as well as being the first example of a bonding interaction residing over four atoms.

The $[TCNE]^- \cdots [TCNE]^-$ interaction does not fulfill the characteristics expected for a van der Waals intermolecular interaction, as they are solely based on the instantaneous dipolar interactions among the electrons of different molecular fragments. This situation is only found for closed-shell molecules (or ions) that have no charge and sizable multipoles. The electronic structure of these interactions can be represented by a diagram in which the doubly occupied orbitals of one fragment overlap with those from the other, and the bonding and antibonding supramolecular orbitals resulting are both doubly occupied (**7a**). The interaction is strongest when the fragment orbitals that overlap are lone pair orbitals located on one of a few atoms. The van der Waals interactions are much weaker when the doubly occupied orbitals that overlap are molecular orbitals spread over the whole molecule, as in the interactions involving peripheral H atoms, as between H_2 molecules or alkanes; in the latter case, the interactions could also be considered as coming from C–H ··· C interactions.[21] The dominant energetic term in the van der Waals interactions is the so-called dispersion component.[22]

0947-6539/02/0821-4898 $ 20.00+.50/0 *Chem. Eur. J.* **2002**, *8*, No. 21

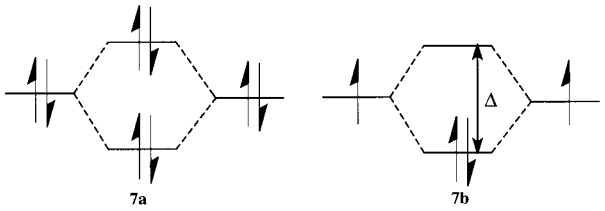

7a **7b**

When we compare the $[TCNE]^- \cdots [TCNE]^-$ interaction with that expected for a van der Waals interaction, several differences arise. First, the electronic structure of the $[TCNE]^- \cdots [TCNE]^-$ interaction (**7b**) presents an open-shell character, thus capable of generating a bonding term (E_{bond}) when overlapped with a similar orbital. At the same time, as noted above, the $[TCNE]^- \cdots [TCNE]^-$ interaction is dominated by an electrostatic (E_{coul}) component, associated to the anionic nature of the $[TCNE]^-$ fragments. Hence, the $[TCNE]^- \cdots [TCNE]^-$ interaction cannot be van der Waals′ in nature. (Note that the $[TCNE]^- \cdots [TCNE]^-$ interaction also cannot be considered purely ionic because although dominated by the electrostatic term, the ionic interactions have $E_{bond} = 0$.) Finally, they are not normal covalent bonds, as the electrostatic term (E_{coul}) plays an important role in defining the shape of the potential-energy curve of the interaction (vide infra). Thus, the two-electron four-center $\pi^* - \pi^*$ interaction found within a $[TCNE]_2^{2-}$ dimer has a mixture of coulombic and covalent character.

The S_o and S_1 diabatic curves cross in the region between the minimum and the dissociation geometries. If the two diabatic curves are allowed to interact, as occurs in accurate ab initio methods, an adiabatic curve that describes the real physical situation is obtained. This adiabatic curve is approximately made of the lowest energy portions of the S_o and S_1 diabatic curves (broken line in Figure 4). When the minimum of the S_o curve is shallow, there is a transition state in the region in which the two diabatics curves cross. However, the barrier for the transition state decreases as the stability of the S_o state increases and with sufficient stability of the S_o state it can disappear, as is the case for most chemical bonds due to their large dissociation energy. Both the UHF or UBL3YP methods allow the interaction between the S_o and S_1 states; that is, they provide adiabatic potential-energy curves for the interaction of the two $[TCNE]^{\bullet -}$ fragments. This is not always the case for RHF or RB3LYP methods. It is possible to determine by UHF or UBL3YP methods the relative importance of the S_o and S_1 components on the singlet adiabatic wavefunction by looking at the occupation numbers of the natural orbitals obtained by diagonalizing the density matrix of the broken symmetry UHF or UBL3YP wavefunctions. If the occupation number of the b_{2u} and b_{1g} orbitals are close to 2 and 0, respectively, the dominant component is closed-shell (i.e., S_o); whereas when the dominant component is the open-shell singlet (i.e., S_1), the occupation numbers are 1 for both orbitals. MCSCF computations on the B3LYP optimum geometries were also performed to check the validity of the B3LYP description as the long-distance minima may have a strong diradical character not properly described by the UHF or UBL3YP methods. Note that this analysis only describes the shape of the E_{bond} component of the total interaction energy between the two $[TCNE]^{\bullet -}$ fragments. However, the minima present in E_{int} are induced by the minima found in the E_{bond} curve, thus showing the importance of the previous qualitative analysis of this component.

Potential-energy curve of the $[TCNE]_2^{2-}$ dimer: An initial potential-energy surface of the $[TCNE]_2^{2-}$ dimers can be obtained by testing if the experimental energy structures are a minimum on the potential-energy surface. Thus, starting from the experimental structures of the $[TCNE]_2^{2-}$ dimers, a preliminary optimization of the closed-shell singlet potential-energy surface was done at the RHF and RB3LYP levels by using the STO-3G, 6-31 + G and 6-31 + G(d) basis sets. The computed minimum-energy structures were close to the experimental geometry in all cases for each of the S_t, L_c, and L_t groups of conformers. The interaction energies and optimum values of the *r* parameter are not strongly dependent of the basis set used, Table 4. A vibrational analysis of the optimized $[TCNE]_2^{2-}$ dimer geometries verifies the minimum-energy nature of these structures as no imaginary frequencies are present. It is worth noting that these minima are all higher in energy than the dissociated products by 58.7, 60.3, and 72.8 kcal mol^{-1} for S_t, L_c, and L_t groups, respectively, that is, the $[TCNE]_2^{2-}$ dimers are metastable at the RB3LYP/6-31 + G level.

Table 4. Interaction energies, $E_{int} = E_{coul} + E_{bond}$ in [kcal mol^{-1}] relative to two isolated $[TCNE]^-$ monomers and the value of the *r* parameter [in italics, in Å] for the optimum energy structure of the S_t, L_c, and L_t conformers of the $TCNE^-$ dimers, as a function of method and basis-set.

Conformer	UHF/6–31 + G(d)	B3LYP/6–31 + G	B3LYP/6–31 + G(d)
S_t	72.1	72.8	69.5
	1.62	*1.71*	*1.70*
L_c	94.9	60.3	60.3
	2.74	*3.13*	*3.04*
L_t	[a]	58.7	59.2
	[a]	*3.26*	*3.19*

[a] No minimum was found.

We also evaluated the shape of potential-energy surface of the $[TCNE]_2^{2-}$ dimer in regions far from the previous minimum-energy points by looking at the change in the interaction energy as a function of *r* while allowing all other dimer geometrical parameters to be fully optimized. We first performed such a search for $1 \le r \le 5$ Å for the closed-shell singlet potential-energy surface (S_o) at the RB3LYP/6-31 + G level, that is, enforcing the double occupancy of the orbitals. Two separate curves were computed for the L_c, and L_t conformers (Figure 5). The only minima for the S_t, L_c, and L_t minimum-energy conformers were as described before. The shape of these two curves indicates that $E_{coul} > E_{bond}$ in this case. Although not shown in Figure 5, for $r \gg 5$ Å the interaction between the two anions is always repulsive, approaching the shape expected for the Coulombic interaction between two point anions as the distance increases; this goes to zero at infinity.

  0947-6539/02/0821-4899 $ 20.00+.50/0

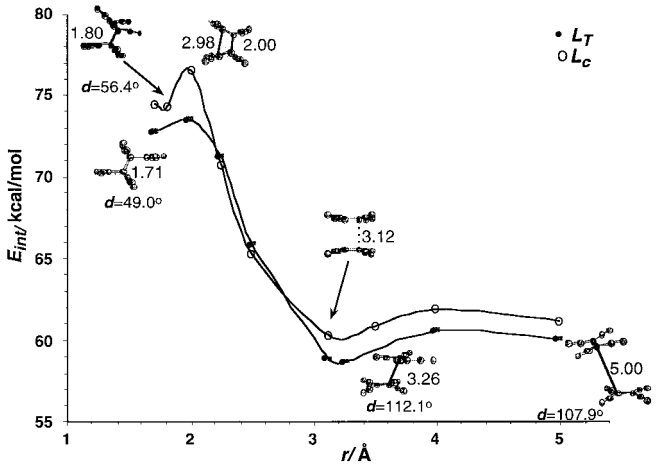

Figure 5. Computed adiabatic potential-energy surface along *r*.

For topological reasons, the presence of minima in the potential-energy surface requires of the presence of a transition state (TS) connecting each of these minima. The TS connecting the S_t and L_t minima is around the region of maximum energy connecting those conformers, Figure 6. Also

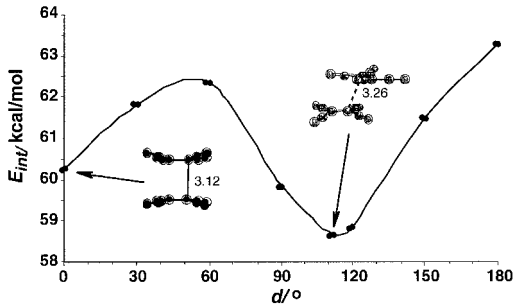

Figure 6. Potential-energy curve for the L_t to L_c transformation along *d*.

shown is the maximum energy region connecting the S_t and L_c minimum. The TS that connects the L_t and L_c conformers can only be seen by computing the change in energy as the dihedral angle *d* was forced to change from 0 to 180°, while the other parameters were fully optimized. The resulting curve connects the optimum geometry of the L_c conformer ($d = 0°$) with that for the L_t conformer ($d = 120°$) through a low barrier transition state of ~ 3 kcal mol^{-1} (see Figure 6).

The existence of these transition states originates from the bond-making/bond-breaking process required to go from one conformer to other, and can only be fully understood once the bonding interactions in each conformer have been properly established. The presence of intradimer bonding interactions in the L_c and L_t conformers can be evaluated with the help of the atoms in molecules (AIM) methodology.[23] This methodology rigorously identifies the presence of bonding interactions by searching for the presence of $(3, -1)$ bond critical points in the electron density. Mathematically, bond critical points are locations (with coordinates r_c) in the electron density space in which the gradient of the electron density is zero, and the Hessian of the density presents two negative and one positive eigenvalues (each identified as λ_i). Critical points associated with chemical bonds (either covalent or weakly ionic in nature) can be distinguished from those associated with *intermolecular* bonds (hydrogen or van der Waals bonds).[23] Chemical bonds have a negative Laplacian [$\nabla^2\rho(r_c)$, defined as the sum of the Hessian eigenvalues], large values of the density at the critical point [$\rho(r_c)$], large $|\lambda_1|/\lambda_3$ ratios, and the lowest and highest eigenvalues of the electron density Hessian (i.e., the lowest and highest curvature of the density at the critical point). In contrast, intermolecular bonds have a positive Laplacian, small values of the density at the critical point, and small $|\lambda_1|/\lambda_3$ ratios. When the intermolecular critical point connects atoms A and B, then the A···B contact is a van der Waals bond.[21b] Note that some controversy exists as to whether the existence of a $(3, -1)$ bond critical point is sufficient condition or just a necessary condition for the presence of a bond, as some authors dispute that only these $(3, -1)$ critical points associated to energetically stable interactions can be considered as bonds.[24]

The $(3, -1)$ bond critical points between the two $[TCNE]^-$ units for each of the L_t, L_c, and S_t minimum-energy conformations found in the RB3LYP were located (Figure 7,

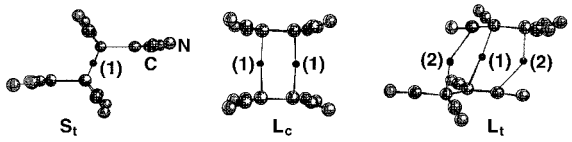

Figure 7. Position of the bond critical points in the S and L conformers of the S_t, L_c, and L_t groups of π-$[TCNE]_2^{2-}$ dimers.

Table 5). The solid lines in this figure, called bond paths, link bond critical points with the atoms of each $[TCNE]^{\bullet-}$ fragment involved in the bond. Note that the bonding in the L_c and L_t conformers is not the same, thus justifying the existence of a transition state between these two conformers as bonds are being broken and created when passing from one conformer to the other. In the L_c structure there are two equivalent bond critical points connecting the central C atoms of each unit (Figure 7). These bonding interactions are the ones expected for structure **3**. However, in the L_t conformer, besides the CC bond critical point between central C atoms (type 1 in Figure 7), there are two equivalent NC bonds linking the C atom of a cyano group in one fragment, to a central C atom of the other fragment (type 2 in Figure 7). The intermolecular N–C bond originates from the presence of unpaired electron density on the CN atoms, as found in the resonant form **6e**. Therefore, to convert from the L_c to the L_t

Table 5. Characteristic properties of the bond critical points of each complex. When more than one critical point is present, they are identified by a number consistent with that given in Figure 8, under the column #CP. For each point the density at the point [$\rho(r_c)$], the Laplacian [$\nabla^2\rho(r_c)$], and the ratio $|\lambda_1|/\lambda_3$ are given (see text for definitions).

Conformer	#CP	$\rho(r_c)$	$\nabla^2\rho(r_c)$	$\lvert\lambda_1\rvert/\lambda_3$
S_t	1	0.167	−0.178	764
L_c	1	0.012	0.023	0.201
L_t	1	0.011	0.021	0.200
	2	0.009	0.021	0.184

0947-6539/02/0821-4900 $ 20.00+.50/0 *Chem. Eur. J.* **2002**, *8*, No. 21

conformer an intradimer central C–C bond (type 1) breaks, while two new C–N bonds (type 2) form. This bond making/breaking process requires the presence of barriers for the transformation. Similarly, the formation of the S_t conformer from the L_t or L_c conformers requires breaking one of the $C(sp^2)$–$C(sp^2)$ or $C(sp^2)$–N bonds and the formation of a $C(sp^3)$–$C(sp^3)$ bond. Therefore, a barrier separating the S and L conformers should exist, as found (Figure 6). The existence of a minimum in the potential-energy surface for the short distance σ-dimer (**2**) can be associated with the overlap between the sp^3 orbitals of the $C(sp^3)$–$C(sp^3)$ bonds when compared to the p–p overlap found in the intermolecular $C(sp^2)$–$C(sp^2)$ bonds. When the effect of the increase in the coulombic repulsion, due to the shorter intradimer distance, is added, the net effect is a destabilization of the S_t conformer relative to the L conformers.

The quantitative features of the critical points of the L_t, L_c, and S_t minimum-energy conformers, that is, electron density, Laplacian, and $|\lambda_1|/\lambda_3$ ratio for each bond critical point(s), are summarized in Table 5. The Laplacian of the critical point is negative for the S_t conformer, but is positive for both L conformers, and the $|\lambda_1|/\lambda_3$ ratio is large for the S_t conformer, but small for the L conformers. These are characteristic of the presence of a covalent bonding interaction between the two units in the S_t conformer, while also indicating the presence of two or three intermolecular bonding interactions (hydrogen-bonded or van der Waals in nature) between the two units of the L_c and L_t conformations. As the bond path directly connects heavy atoms, the intermolecular interaction is identified as a van der Waals bond. However, the bonding interactions in the L_t and L_c conformers cannot be van der Waals interactions because, as discussed above, these bonding interactions originate from the interaction of singly occupied orbitals (SOMO; **7a**; Figure 3) and not from an interaction of doubly-occupied orbitals, as is the case in van der Waals bonds (**7b**). The AIM analysis provides the Laplacian expected for an intermolecular bond, probably because of the large intermolecular C···C distance between the fragments in the L_t and L_c conformers. Note that the existence of bond critical points is only one of the necessary conditions for the existence of the bonds; it is also necessary that the aggregate formed as a consequence of the new bond is a stable one. Both the RHF and B3LYP methods predict that all conformers are metastable, but further studies with more accurate methods are required before reaching a final conclusion (vide infra).

The imposition of doubly occupied orbitals implicit in the RB3LYP method may be an nonphysical restriction, particularly at the large distances found for the minima of the L_c and L_t conformers, thus making it neccesary the use of more accurate ab initio methods for the study of these dimers. The UB3LYP total energy of the L_c and L_t conformers at the RB3LYP optimum geometry was computed for both the closed- and open-shell singlets; the latter obtained by using broken symmetry (BS). At this geometry one can get an indication of the physical nature of the double occupancy by looking at the occupation number of the natural orbitals of that wavefunction. This was done for the b_{2u} and b_{1g} dimer orbitals arising from the SOMO orbitals of each $[TCNE]^{\bullet -}$, and also the b_{2u} antibonding orbital next in stability to the b_{1g} orbital. The occupation numbers of the b_{2u}, b_{1g}, and b_{2u} orbitals in the L_c conformer are 2.0, 1.7, and 0.3 e^-, respectively, and 2.0, 1.5, and 0.5 e^-, respectively, in the L_t conformer. These two sets of numbers indicate a non-negligible weight of the S_1 open-shell wavefunction, which requires non-doubly occupied orbitals for its description. For comparison, the S_t conformer has the same occupation numbers of 2.0, 0.0, and 0.0 e^-, indicating a negligible weight of the S_1 open-shell component in this case. Given the non-negligible weight of the S_1 state in the electronic wavefunctions of the L_c and L_t conformers, the shape of the potential-energy curve along the *r* coordinate was computed at the UB3LYP level, at the optimum geometry found in the closed-shell RB3LYP calculations (Figure 8). At short distances the UB3LYP curve

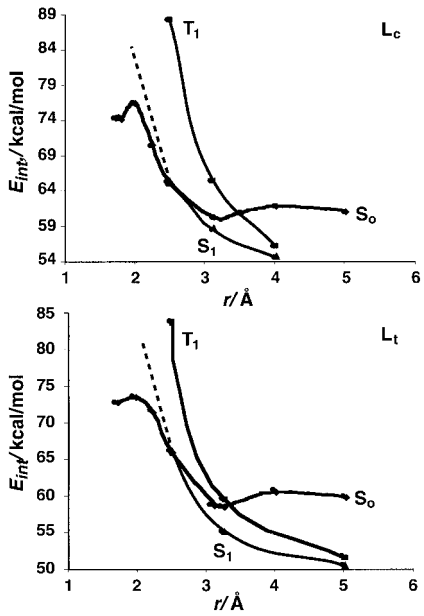

Figure 8. Closed-shell $^1A_{1g}$ singlet (S_o), open-shell $^1B_{1u}$ singlet (S_1), and $^3B_{1u}$ triplet curves (T_1) along *r* for the L_c and L_t groups of π-$[TCNE]_2^{2-}$ dimers. The closed shell S_o curves are computed at the RB3LYP level, the T_1 curves are computed at the UB3LYP level, and the S_1 curves are computed as broken symmetry singlet (SBS) curves.

collapses into the closed-shell RB3LYP curve, as expected. However, at distances larger than 2.5 Å, the S_1 state becomes important and the BS curve becomes more stable. The BS curve does not show any minima for the L_c and L_t conformers. Consequently, the minimum computed at the RB3LYP level is an artifact, that is, a consequence of the doubly occupancy restriction imposed to the orbitals. The triplet-state curve at the same geometry is also plotted in Figure 8. As the triplet curve lies higher in energy than the SBS singlet, the ground state of the L groups of dimers is a singlet, in good agreement with experiment.

The results of the UB3LYP broken symmetry calculations were confirmed by MCSCF(6,4) computations on the same geometries by using a complete active space made of six electrons and four orbitals. The six electrons present are those placed in the π and π* orbitals of each $[TCNE]^-$ fragment (three per fragment), and the four orbitals are the π and π*

  0947-6539/02/0821-4901 $ 20.00+.50/0

from each fragment (two per fragment). These calculations were carried out using the 6-31 + G basis set previously used in the UB3LYP calculations. For any given geometry, the population of the b_{2u}, b_{1g}, and b_{2u} orbitals in these MCSCF calculations differ by $< \pm 0.1\ e^-$ with respect to the B3LYP results for the same geometry. The shapes of the S_o and S_1 curves at the MCSCF level are also similar to those found at the UB3LYP level. Furthermore, a full optimization of the geometry of the L_c and L_t conformers at the MCSCF(6,4) level, starting from the RB3LYP minimum conformations, produces dissociation into the $[TCNE]^-$ fragments. Therefore, both the UB3LYP and MCSCF results indicate that the L_c and L_t conformers *are not minimum-energy structures in their potential-energy surface*. The existence of minima at the RB3LYP level for the L conformers is a consequence of the double occupancy restriction imposed in this method. Hence, the presence of $[TCNE]_2^{2-}$ dimers with either the L_c or the L_t conformation, as observed, must result from the attractive cation – $[TCNE]_2^{2-}$ electrostatic interactions that overcompensate the repulsive $[TCNE]^- \cdots [TCNE]^-$ electrostatic interaction.

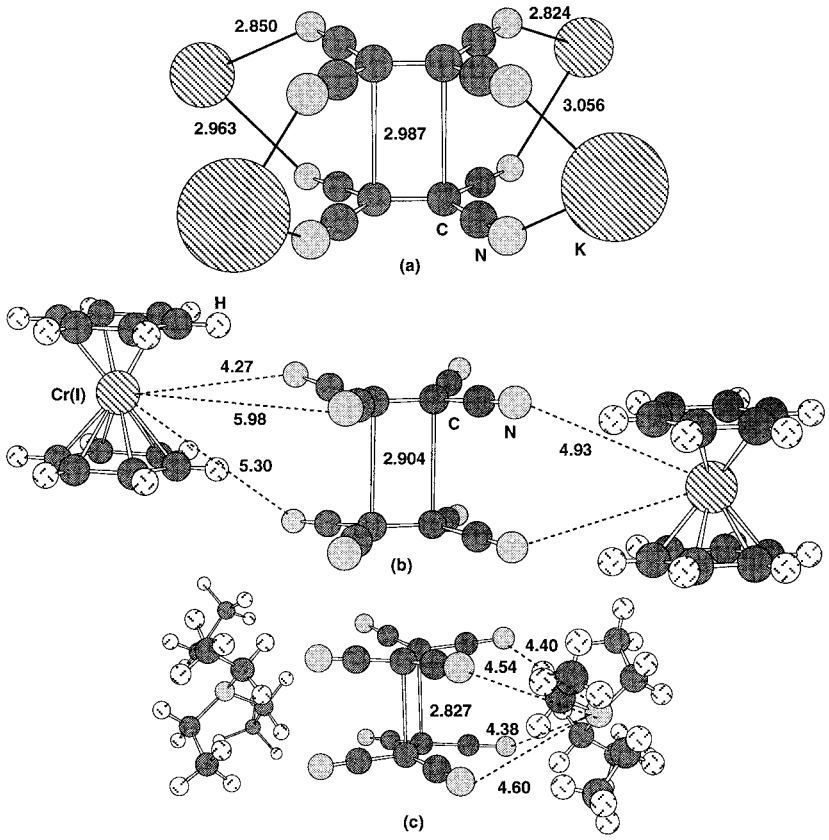

Figure 9. Geometry of the neutral (cation)$_2$[TCNE]$_2$ unit used to compute the energetic of the intermolecular interaction in the a) $K_2[TCNE]_2(glyme)_2$,[7d] b) $[Cr^I(C_6H_6)]_2[TCNE]_2$,[7b] and c) $[Et_4N]_2[TCNE]_2$.[7i] The key intermolecular distances between the fragments are noted in Å. This unit has a net charge of zero.

Computational studies on $K_2[TCNE]_2(glyme)_2$, $[NEt_4]_2[TCNE]_2$, and $[Cr(C_6H_6)_2]_2[TCNE]_2$ show these cation – anion electrostatic interactions do not depend on the size or type of the cation. $K_2[TCNE]_2(glyme)_2$ possesses two μ_4-$[TCNE]_2^{2-}$ units (Table 2) each bound to two K^+ ions (2.905 ± 0.055 Å from the N's nominally midway between the two parallel $[TCNE]^-$ planes; Figure 9a), and two neutral glyme molecules also bound to the K^+ ions.[7d] The intradimer CC separation of ~3.0 Å is significantly less than the sum of the van der Waals radii of 3.4 Å[25, 26a] with a CC interdimer separation of ~4.5 Å. At the UHF/6-31 + G(2d,2p) level the $[TCNE]_2^{2-}$ with the short intradimer distance has a 103.0 kcal mol^{-1} repulsive interaction in its lowest triplet state. However, the $K^+ \cdots [TCNE]^-$ interactions within the $K_2[TCNE]_2$ aggregate are attractive by 75.0 kcal mol^{-1}. Thus, although the $[TCNE]_2^{2-}$ dimers are energetically unstable with respect to dissociation, the neutral $K_2[TCNE]_2$ aggregate is stable with respect to dissociation by 158.4 kcal mol^{-1}. This value is close to the average previously found by using ab initio methods for the interactions present in many ionic molecular crystals involving singly charged ions; this is on the order of 200 kcal mol^{-1}.[27]

$[NEt_4]_2[TCNE]_2$[7i] and $[Cr(C_6H_6)_2]_2[TCNE]_2$[7b] have structures with $[TCNE]_2^{2-}$ dimers in which the cations are placed sideways with respect to the anions (Figure 9b,c). The interactions between the fragment for $[NEt_4]_2[TCNE]_2$ and $[Cr(C_6H_6)_2]_2[TCNE]_2$ have been computed for the units shown in Figure 9. At the UHF/6-31 + G(2d,2p) level the $[TCNE]_2^{2-}$ units are repulsive by 83.5 kcal mol^{-1} $[NEt_4]_2[TCNE]_2$ and the $[NEt_4]^+ \cdots [NEt_4]^+$ interactions are repulsive by 19.3 kcal mol^{-1}. In contrast, the $[NEt_4]^+ \cdots [TCNE]^-$ interactions are attractive (by −58.1, −58.0, −66.1, and −66.0 kcal mol^{-1}), and the overall stabilization is −145.2 kcal mol^{-1}, that is, it requires 145.2 kcal mol^{-1} to dissociate the aggregate into its constituent ions. When the same energetic balance is done on the $[Cr(C_6H_6)_2]_2[TCNE]_2$ at the UHF/6-31 + G(2d,2p) level, the $[TCNE]_2^{2-}$ units are repulsive by 79.9 kcal mol^{-1}, as are the $[Cr(C_6H_6)_2]^+ \cdots [Cr(C_6H_6)_2]^+$ interactions by 12.2 kcal mol^{-1}. However, the four $[Cr^I(C_6H_6)_2]^+ \cdots [TCNE]^-$ interactions are attractive by −67.5, −68.5, −57.2, and −24.1 kcal mol^{-1}; thus the overall interaction energy is −125.2 kcal mol^{-1}. Hence, larger cations seem to minimally decrease the stability of $[TCNE]_2^{2-}$ dimers (which decreases from 103.0 kcal mol^{-1} in the K^+ salt, to 83.5 kcal mol^{-1} in the $[NEt_4]^+$ salt, and 79.9 kcal mol^{-1} in the $[Cr(C_6H_6)_2]^+$ salt) as does the net stability, which are 158.4, 145.2, and 125.2 kcal mol^{-1}, respectively.

The results of our computational studies indicate the net charges and their geometrical arrangement are the most important factors that define the strength of the interactions

0947-6539/02/0821-4902 $ 20.00+.50/0 *Chem. Eur. J.* **2002**, *8*, No. 21

in ionic crystals.[27a, 28] Thus, for instance, if the $[Cr(C_6H_6)_2]^+$ ions of Figure 9b are placed perpendicular to the nominal $[TCNE]^-$ planes of the $[TCNE]_2^{2-}$ units, the $[TCNE]_2^{2-}$ unit is unstable with respect to dissociation into two $[TCNE]^{\bullet-}$ moieties. Therefore, despite the strong repulsive intradimer interaction supramolecular $[cation]_2[TCNE]_2$ dimers form, as the cation–anion interactions stabilize the $[TCNE]_2^{2-}$ dimers with a short 2.9 Å intradimer separation. As a consequence of this small separation, the singly occupied (SOMO) π^* orbitals of each $[TCNE]^{\bullet-}$ monomers overlap; this leads to intermolecular bonding and antibonding dimer orbitals separated by a non-negligible energy gap, Δ (**7b**), similar to that observed for energetically stable bonds, for example, H_2.[17] Owing to this gap, the $[TCNE]_2^{2-}$ dimer interactions exhibit all the structural, spectroscopic, and magnetic properties of a bond, as discussed below. Therefore, the intradimer CC bonding within the $[TCNE]_2^{2-}$ dimers is cation-mediated. In contrast, other similar cations, for example, $[N(n\text{Bu})_4]^+$[5c] and $[Fe(C_5Me_5)_2]^+$,[5a] do not stabilize $[TCNE]_2^{2-}$. Note, however, that polymorphs with the $[TCNE]_2^{2-}$ dimers could exist for these cations, although they have not been detected yet.

Electronic structure of $[TCNE]_2^{2-}$ dimers

Experimental evidence of long CC intradimer bonding—electronic absorption spectra: As noted above, although isolated $[TCNE]_2^{2-}$ dimers are not energetically stable with respect to fragmentation, the cation–$[TCNE]_2^{2-}$ interactions stabilizes $[cation]_n[TCNE]_m$ aggregates (e.g., Figure 9), making the aggregate energetically stable with respect to dissociation into fragments. The cation acts as the "glue" which keeps the two $[TCNE]^-$ anions at a distance that enables the orbitals of each fragment to overlap.

Ab initio calculations carried out on the $[TCNE]_2^{2-}$ dimers at the range of distances observed for the S and L conformers show the existence of an energy splitting between the bonding b_{2u} and antibonding b_{1g} orbitals (Δ; **7a**; Figure 3). This $b_{2u}-b_{1g}$ orbital splitting (Δ) gives rises to two singlet states, S_o (arising from the $b_{2u}^2b_{1g}^\circ$ configuration), and the $b_{2u}^1b_{1g}^1$ S_1 configuration, whose energy difference is the source of a new, allowed electronic transition that is observed for $[TCNE]_2^{2-}$ in the visible region of the spectrum. Experimentally, this new absorption is observed in the range of 15000 (667 nm; 1.86 eV) to 18200 cm^{-1} (549 nm; 2.26 eV) [average is 16825 ± 1180 cm^{-1}[29] (594 nm; 2.09 eV)] for nine $[TCNE]_2^{2-}$ dimers (Table 2 and Figure 10); this results in the dimer being purple when viewed by reflected light.

These data are consistent with early studies on nonstructurally characterized M[TCNE] (M = Na, K, Rb, Cs); the results showed that their room-temperature solid-state spectra exhibited new absorptions at $\sim$18500 cm^{-1} (541 nm; 2.29 eV), which were assigned to a charge transfer between two $[TCNE]^{\bullet-}$'s within a dimer.[12] Albeit on the high-energy side of our data, this is consistent with absorptions for structurally characterized $[TCNE]_2^{2-}$ within dimers.

Our preliminary ab initio computational results suggest that the $[TCNE]_2^{2-}$ dimer should be stable in solution at low temperature. The solution spectra of a saturated solution of $[Et_4N]_2[TCNE]_2$ dissolved in 2-methyl tetrahydrofuran (MeTHF) only shows the spectral features typical of yellow $[TCNE]^{\bullet-}$ dissolved in solution (Figure 11a).[15] However, upon rapid cooling to 77 K, such that a transparent deep red frozen glass forms, the absorption characteristic of $[TCNE]^{\bullet-}$ disappears, and new absorptions at 18940 and 26000 cm^{-1} (528 and 385 nm) appear (Figure 11b). Hence, $[TCNE]_2^{2-}$ is thermal chromic. This is consistent with the equilibrium $2[TCNE]^{\bullet-} \rightleftharpoons [TCNE]_2^{2-}$ being shifted to the right with

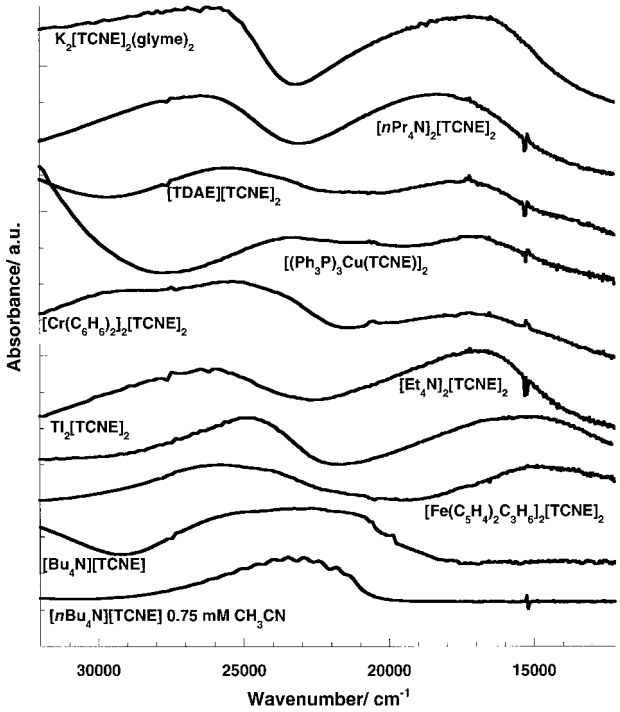

Figure 10. Experimental UV-visible spectra of solid (KBr pellet) $[Et_4N]_2[TCNE]_2$, $[n\text{Pr}_4N]_2[TCNE]_2$, $[n\text{Bu}_4N]_2[TCNE]_2$, $Tl_2[TCNE]_2$, $[TDAE][TCNE]_2$, $[Fe(C_5H_4)_2C_3H_6]_2[TCNE]_2$, $[Cr(C_6H_6)_2]_2[TCNE]_2$, $[Cu(PPh_3)_3(TCNE)]_2$, and $K_2[TCNE]_2(glyme)_2$. The absorptions at $\geq$25000 cm^{-1} are assigned to $[TCNE]^-$ transition as observed for $[n\text{Bu}_4N]_2[TCNE]_2$ in solution (75 mM in MeCN).

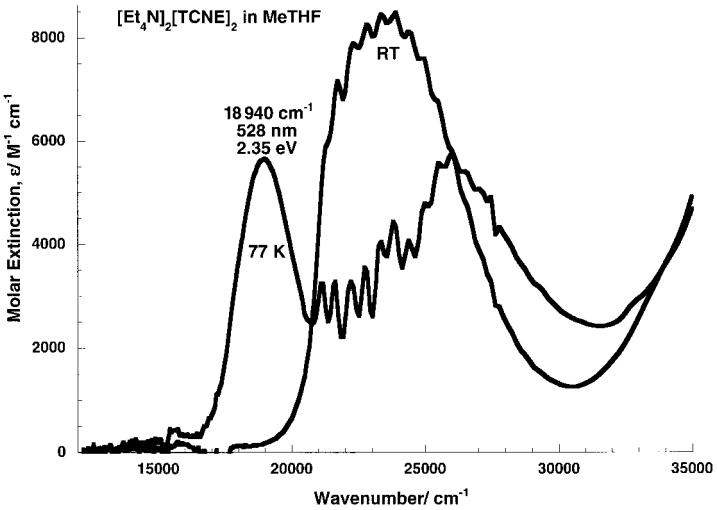

Figure 11. UV-visible electronic absorption spectra of a saturated solution of $[Et_4N]_2[TCNE]_2$ in MeTHF at at room temperature and at 77 K. The data is reported as molar extinction (ε) per mole of $[TCNE]^{\bullet-}$ as a function energy based on $\varepsilon(23375\ cm^{-1}) = 8425\ M^{-1}cm^{-1}$.[15]

decreasing temperature in accord with entropy considerations, such that at 77 K sufficient amounts of the $[TCNE]_2^{2-}$ dimer is present and stable.[30] Similar solution spectra of $[TCNE]_2^{2-}$ as a 2-methyl tetrahydrofuran glass at 77 K were also reported [$\lambda_{max} = 18500\ cm^{-1}$ (540 nm)].[12]

The stronger the intradimer interaction the greater the b_{2u} and b_{1g} orbital splitting (Δ), and the change in the value of Δ with the intradimer separation r for the L_t curve has been estimated by computing the separation Δ'[31] between the singlet ground state S_o (configuration: $b_{2u}^2 b_{1g}^{\circ}$; symmetry: $^1A_{1g}$) and the S_1 excited state (configuration: $b_{2u}^1 b_{1g}^1$; symmetry: $^1B_{1u}$), Figure 4. However, Δ is not a physically observable quantity, and its variation can only detected by the effect that it has on physically observable properties. The $S_o - S_1$ energy difference (Δ') was computed at the CIS/6-31 + G level, a method known to give reasonable values of the separation between states and the UV-visible spectrum.[32] These calculations show that the $S_o - S_1$ (Δ') energy difference increases as r decreases, from a value of $\sim 15000\ cm^{-1}$ (1.86 eV) at 3.3 Å to a value of $22000\ cm^{-1}$ (2.73 eV) when r is 2.8 Å (Figure S2 in the Supporting Information).

Attempts to experimentally observe this trend were unsuccessful, as no correlation was noted when the energy of the lowest energy (ν_{max}) transition (Table 2, Figure 10) is plotted as a function of intradimer separation (r; Figure S3 in the Supporting Information). The lack of a correlation is a consequence of Δ increasing with decreasing r as the overlap increases, while the energy separating the HOMO and LUMO (Δ') decreases with increasing r. In addition to these competing trends, the spatial extent of the two-electron four-center dimer HOMO orbital will change due to polarization by the vastly differing cations and, hence, alter the overlap and Δ and Δ' making simple correlation unlikely. Bulky, distant noninteracting cations such as $[n\mathrm{Pr}_4\mathrm{N}]^+$ or $[\mathrm{Fe}^{III}(C_5H_4)_2C_3H_6]^+$ will polarize the orbital differently than $[TDAE]^{2+}$ or point-charge cations (e.g., Tl^+, K^+) that have strong electrostatic interactions with the $[TCNE]_2^{2-}$ dimer. Additionally, covalent bonding of a nitrile of the $[TCNE]_2^{2-}$ dimer to a cation, as occurs for $Cu(PPh_3)_3[TCNE]$,[7a] should also affect the extent of overlap within the dimer. Thus, the cation interferes too much with the individual orbitals of $[TCNE]_2^{2-}$ dimer and prevents a simple interpretation of the $\Delta'(r)$ data. This is observed as dimers with almost identical intradimer separations distances have significantly different transition energies, for example, $[n\mathrm{Pr}_4\mathrm{N}]_2[TCNE]_2$ (r = 2.871 Å) absorbs at $18300\ cm^{-1}$ (546 nm), while $Tl_2[TCNE]_2$ (r = 2.874 Å) absorbs at $15100\ cm^{-1}$ (623 nm).

Hybridization: The change in the geometry of the $[TCNE]^-$ fragments as the intradimer separation (r) decreases leads to change in the hybridization around the central carbons for the L_c and L_t groups of $[TCNE]_2^{2-}$ dimers. The central CC distance increases with decreasing r and, simultaneously, the dihedral angle (d) increases from 90 to 120°. This corresponds to a shift from sp^2 towards sp^3 hybridization at the two central carbon of each $[TCNE]^-$ fragment. The change in hybridization of the central carbons as the intradimer distance decreases is followed by changes in the *trans*-NC-C-C-CN angle, while the CN's move out of the nominal $[TCNE]^-$ plane away from the $[TCNE]_2^{2-}$ dimer's center of symmetry by 2.3° to 6.6° (average = 5.0 ± 1.3°), Table 2. The bending away of the nitrile groups from the center of the L_c $[TCNE]_2^{2-}$ dimer is illustrated in Figure 12 (top). Based upon the average bending

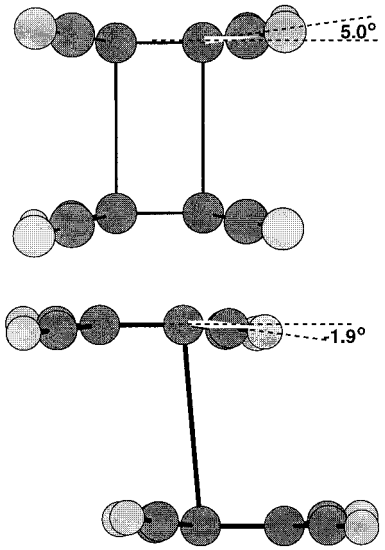

Figure 12. Structure of $[Et_4N]_2[TCNE]_2$ exhibiting how the nitriles bend away the center of the dimer for the L_c group of $[TCNE]_2^{2-}$ dimers by an average of 5° (corresponding to a hybridization of 2.17; top), and α-[TTF][TCNE] exhibiting that the nitriles bend toward the center of the dimer for the L_t group of $[TCNE]_2^{2-}$ dimers by an average of −1.9° (corresponding to a hybridization of 2.06; bottom).

of the nitriles away form the center of the L_c $[TCNE]_2^{2-}$ dimer by 5.0°, its average C_1-C_3-C_4-CN dihedral angle (see structure **4**) is 95°. Assuming a linear relationship between 90° dihedral angle for sp^2 and 120° for sp^3 hybridization,[26b] the hybridization for the central carbons of the $[TCNE]_2^{2-}$ dimers is estimated to be 2.17. This change is also observed in the optimized geometries in Figure 2, and is the expected when a CC bond is formed with an sp^2 C atom. In contrast, the nitriles bend toward the $[TCNE]_2^{2-}$ dimer center of symmetry for the L_t group (Figure 12, bottom) by 1.0° to 2.8° (average = 1.9°), Table 2. The average 1.9° deviation from planarity corresponds to a dihedral angle of 91.9°, and the hybridization for the central carbons of the L_t group of $[TCNE]_2^{2-}$ dimers is estimated to be 2.06.[26b] This bending toward the dimer's center is not understood and is the subject of further studies.

Vibrational absorption spectra: The different bonding interactions are also manifest in the IR spectra—that of the dimer differs with respect to its fragments. Thus, the change in the IR absorption frequencies when going from the monomer to the dimer, and in particular the changes in the C≡N stretching frequencies, have been analyzed. Table 6 lists the $\nu_{C\equiv N}$ harmonic stretching frequencies computed at the RB3LYP/6-31 + G level, and their IR intensities. The intensities and frequencies are in reasonablly good agreement with the experimental values given in Table 2, considering that the computed values were obtained within the harmonic approximation. $[TCNE]^{\bullet -}$ has two strong[15, 33] computed $\nu_{C\equiv N}$ vibrations at $\sim 2200\ cm^{-1}$; these are experimentally observed at

0947-6539/02/0821-4904 $ 20.00+.50/0 *Chem. Eur. J.* **2002**, *8*, No. 21

Table 6. ν_{CN} stretching frequencies [cm^{-1}] and infrared intensities [in parenthesis, km mol^{-1}] computed for the $[TCNE]^{\bullet-}$ monomer and dimer at the B3LYP/6–31+G level.

$[TCNE]^{\bullet-}$		S_t		L_c		L_t	
2168	(0)	2165	(0)	2190	(0)	2180	(499)
2180	(442)	2168	(881)	2191	(0)	2184	(33)
2227	(189)	2202	(468)	2201	(0)	2191	(402)
2235	(0)	2210	(0)	2203	(669)	2196	(427)
		2293	(0)	2203	(1517)	2204	(1577)
		2293	(0)	2235	(305)	2235	(139)
		2296	(18)	2240	(0)	2237	(129)
		2299	(12)	2243	(0)	2243	(2)

2183 and 2144 cm^{-1} (Figure 13).[5a, 15] In contrast, L_c π-$[TCNE]_2^{2-}$ is computed at the RB3LYP/6-31+G level to have three $\nu_{C\equiv N}$ vibrations indicative of bonding interactions

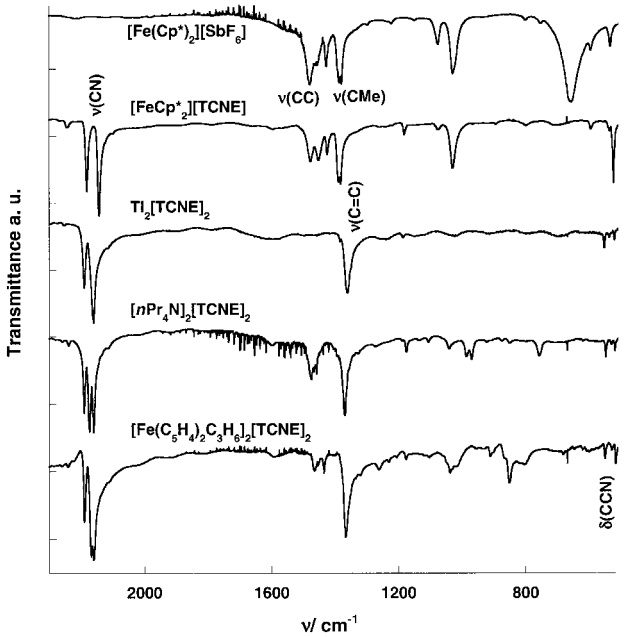

Figure 13. The IR spectra of $[Fe(C_5Me_5)_2][SbF_6]$, $[Fe(C_5Me_5)_2][TCNE]$, $Tl_2[TCNE]_2$, $[nPr_4N]_2[TCNE]_2$, and $[Fe(C_5H_4)_2C_3H_6]_2[TCNE]_2$ as KBr pellets. The IR spectra show the spectra of $[TCNE]^{\bullet-}$ as the $[Fe(C_5Me_5)_2]^+$ salt, which also has the IR spectrum of the $[Fe(C_5Me_5)_2]^+$ cation.

between the two $[TCNE]^{\bullet-}$ fragments (Figure 13). This is in accord with the average observed $\nu_{C\equiv N}$ absorptions of 2191 ± 2 (m), 2173 ± 3 (s), and 2162 ± 3 cm^{-1} (s) for eleven $[TCNE]_2^{2-}$ dimers structurally characterized and for which the IR spectra are available (Table 2). These values differ from those observed for group L_t [2216 ± 2 (m), 2197 ± 3 (m), and 2180 ± 4 cm^{-1} (m)] and S_t [2215 ± 4 (m), 2157 ± 3 (s), and 2107 ± 4 cm^{-1} (w)].

Furthermore, a characteristic IR absorption at ~ 1400 cm^{-1} not observed for $[TCNE]^{\bullet-}$, is predicted to be observed for π-$[TCNE]_2^{2-}$. This new 1400 cm^{-1} absorption is due to the antisymmetric combination of the intrafragment CC stretches of each fragment central CC bond; this absorption becomes allowed and gains intensity as a result of electron-vibrational coupling as the center of symmetry moves from the center of CC bond in an isolated $[TCNE]^{\bullet-}$ to the center of the $[TCNE]_2^{2-}$ dimer.[34] This absorption occurs at 1364 ± 3 cm^{-1} (s) for the eleven $[TCNE]_2^{2-}$ dimers listed in Table 2, for which the IR spectra are available. Hence, the $\nu_{C=C}$ absorption calculated to occur at ~ 1400 cm^{-1} is observed at 1364 ± 3 cm^{-1} for group L_c π-$[TCNE]_2^{2-}$ dimers. Although only Raman active, this $\nu_{C=C}$ absorption occurs at 1558 cm^{-1} for TCNE and shifts to 1421 cm^{-1} for $[TCNE]^{\bullet-}$ and with the change in location of the center of symmetry it becomes IR active and shifts to 1364 cm^{-1} for group L_c π-$[TCNE]_2^{2-}$ dimers, further reflecting a reduced central CC bond order and a weaker central CC bond. This trend is further observed for the S_t and L_t groups of $[TCNE]_2^{2-}$ dimers in which the central CC absorption is assigned to a band at 1209 ± 9 (w) and 1385 ± 1 cm^{-1} (vs), respectively.

In addition, the δ_{C-CN} bending absorption that occurs at 521 ± 1 cm^{-1} (m) for TCNE and $[TCNE]^{\bullet-}$ splits into three absorptions for the L_c and L_t groups of π-$[TCNE]_2^{2-}$ dimers. These new features occur as weak absorptions at 549 ± 2 (w), 530 ± 4 (w), and 516 ± 3 cm^{-1} (w) for the L_c group; at 557 ± 1 (w), 535 ± 5 (w), and 508 ± 3 cm^{-1} (w), for the S_t group; and at 586 ± 3 (w), 535 ± 1 (w), and 520 ± 1 cm^{-1} (w) for the L_t group.

Thus, the L_c group of π-$[TCNE]_2^{2-}$ dimers can be experimentally identified by 1) an additional strong $\nu_{C\equiv N}$ absorbance, 2) the shift of the three $\nu_{C\equiv N}$ absorptions towards higher frequencies, 3) new absorption at 1364 cm^{-1}, and 4) splitting of the 521 cm^{-1} $\delta_{C\text{-}CN}$ absorption into three weaker bands at 549, 530, and 516 cm^{-1}. In the S_t dimer, the calculated frequency of this absorption decreases to 1200 cm^{-1} and its intensity decreases by a factor of five of that found in the L conformers. Furthermore, the $\nu_{C\equiv N}$ vibrations for the S_t group of $[TCNE]_2^{2-}$ dimers occur at 2215 (m), 2157 (s), and 2107 cm^{-1} (w); these are distinct from both the L_c and L_t groups of $[TCNE]_2^{2-}$ dimers.

Magnetic properties of the $[TCNE]_2^{2-}$ dimers: When $S = 1/2$ doublet $[TCNE]^{\bullet-}$ fragments approach each other to form the π-$[TCNE]_2^{2-}$ dimer, $\Delta(r)$ and the triplet–singlet (S–T) separation increases. UB3LYP/6-31+G calculations show (Figure 8) that the unpaired electrons of each $[TCNE]^{\bullet-}$ fragment couple antiferromagnetically into a singlet state, which is the ground state at all distances. This state, however, changes in character from being mostly S_1 at large distance into S_o at short distances. These results indicate that the triplet is always higher in energy with respect to either the closed- or open-shell singlet states. The triplet–singlet energy difference is 5.19 and 0.80 kcal mol^{-1} for the L_t and L_c optimum geometries, respectively (Table 7), but lies at 70.9 kcal mol^{-1} above the closed-shell singlet state for the S_t conformer. However, it was impossible to compute a broken symmetry estimate for the S_t geometry as the SCF method always reverted to the closed-shell solution. The result of these calculations were confirmed by MCSCF(6,4) calculations.

The predicted singlet ground state was experimentally verified by the temperature-dependence magnetic susceptibility in the range of 2 to 350 K for $[Et_4N]_2[TCNE]_2$,[7i] $[nPr_4N]_2[TCNE]_2$,[7m] and $[(Me_2N)_2CC(NMe_2)_2][TCNE]_2$, [TDAE][TCNE]$_2$.[7g] Likewise, more sensitive EPR studies up to 380 K for $[Et_4N]_2[TCNE]_2$ did not show evidence for population of the triplet state. Hence, only diamagnetic-like

Table 7. Summary of the structural and spectroscopic properties of the S_t, L_t, and L_c groups of $[TCNE]_2^{2-}$ dimers (**4**).

	TCNE°	$[TCNE]^{\bullet-}$	S_t	L_c	L_t
Structurally characterized	1	many	2	13	2
dihedral angle, average d [°]	–	–	179.94 ± 0.02	1.65 ± 4.1	179.87 ± 0.06
intradimer CC, average r [Å]	–	–	1.61 ± 0.01	2.90 ± 0.05[a]	3.50 ± 0.04[b]
average intradimer separation [Å]	–	–	–	2.90 ± 0.05[a]	3.47 ± 0.04[b]
average central CC bond [Å]	1.357[14b]	1.39[15]	1.61 ± 0.01	1.405 ± 0.03[f]	1.399 ± 0.002
average NC-C-CN angle [°][c]	116.2[14b]	117.7[15]	118.5[d][15]	118.4	118.6
average CN displacement [°]	0	0	–	5.0 ± 1.3	-1.9 ± 0.9[g]
central C hybridization	sp^2	sp^2	sp^3	$sp^{2.17}$	$sp^{2.06}$
$\nu_{C\equiv N}$ (IR) [cm^{-1}]	2262 ± 1 (m)	2183 ± 1 (m)	2215 ± 4 (m)	2191 ± 2 (m)	2216 ± 2 (m)
	2229 ± 1 (w)	2144 ± 1 (m)	2157 ± 3 (s)	2173 ± 3 (s)	2197 ± 3 (s)
	2215 ± 1 (vw)		2107 ± 4 (w)	2162 ± 3 (s)	2180 ± 4 (m)
ν_{C-C} (IR) [cm^{-1}]	1568 ± 2[e]	1421 ± 1[e]	1209 ± 9 w	1364 ± 3 s	1385 ± 1 vs
ν_{C-CN} (IR) [cm^{-1}]	522 ± 1 (m)	521 ± 1 (m)	557 ± 1 (w)	549 ± 2 (w)	586 ± 3 (w)
			535 ± 5 (w)	530 ± 4 (w)	535 ± 1 (w)
			508 ± 3 (w)	516 ± 5 (w)	520 ± 1 (w)
$^1A_{1g} \rightarrow {}^1B_{1u}$, average Δ [cm^{-1}]	-	-	-	16825 ± 1180	
spin multiplicity	singlet	doublet	singlet	singlet	singlet

[a] Eclipsed. [b] Noneclipsed. [c] Not metal bound. [d] Terminal nitriles are metal bound. [e] Raman active (IR forbidden). [f] Excludes μ_{16}-$[TCNE]_2^{2-}$ dimers. [g] Negative value indicates bending toward the center of the dimer.

behavior was observed. This is consistent with the singlet state being the ground state and the only state that is thermally populated at room temperature.

Conclusion

Three groups of $[TCNE]_2^{2-}$ dimers (**4**; S_t, L_t, and L_c; Figure 1), characterized by the intradimer separation (r) and its dihedral angle (d), have been experimentally reported, Table 2. Each dimer has a singlet ground state, but has distinguishing structural and spectroscopic features (Table 7). With respect to $[TCNE]^{\bullet-}$, the L_c group of π-$[TCNE]_2^{2-}$ dimers can be experimentally identified by 1) an additional strong $\nu_{C\equiv N}$ absorbance; 2) the shift of the three $\nu_{C\equiv N}$ absorptions toward higher frequencies and are observed at 2191 ± 2 (m), 2173 ± 3 (s), and 2162 ± 3 cm^{-1} (s); 3) new absorption assigned to $\nu_{C=C}$ at 1364 ± 3 cm^{-1} (s); and 4) splitting of the ν_{C-CN} absorption with peaks at 549 ± 2 (w), 530 ± 4 (w), and 516 ± 5 cm^{-1} (w). Additionally, the L_t group of π-$[TCNE]_2^{2-}$ dimers can be experimentally identified by 1) an additional strong $\nu_{C\equiv N}$ absorbance; 2) the shift of the three $\nu_{C\equiv N}$ absorptions toward higher frequencies and are observed at 2216 ± 2 (m), 2197 ± 3 (s), and 2180 ± 4 cm^{-1} (s); 3) new absorption assigned to $\nu_{C=C}$ at 1385 ± 1 cm^{-1} (s); and 4) splitting of the ν_{C-CN} absorption with peaks at 586 ± 3 (w), 535 ± 1 (w), and 520 ± 1 cm^{-1} (w). Furthermore, in the solid state the L_c group of $[TCNE]_2^{2-}$ dimers exhibit a new UV-visible feature at 16825 ± 1180 cm^{-1} (594 nm; 2.09 eV) assigned to the intradimer $^1A_{1g} \rightarrow {}^1B_{1g}$ transition; this band is shifted to 18940 cm^{-1} (528 nm; 2.35 eV) in MeTHF at 77 K for $\{[Et_4N]^+\}_2[TCNE]_2^{2-}$.

The observed physical properties of the L_c group of π-$[TCNE]_2^{2-}$ dimer are consistent with those expected from the formation of a covalent CC bonding interaction between the two $[TCNE]^-$ monomers. Due to the repulsive electrostatic interactions, however, the $[TCNE]^- \cdots [TCNE]^-$ interactions are energetically unstable in the absence of charge-neutralizing cations. Hence, neutral $(cation)_2[TCNE]_2$ is energetically stable due to the attractive electrostatic cation $\cdots$ $[TCNE]^-$ interactions, which exceed the repulsive electrostatic $[TCNE]^- \cdots [TCNE]^-$ interactions. This cation-mediated stabilization enables the direct overlap of the SOMOs of two $[TCNE]^-$ monomers over four carbon atoms and, thus, is responsible for the existence of cation-mediated $\pi^* - \pi^*$ CC covalent bonding that occurs in the $(cation)_2[TCNE]_2$ aggregates.[35] This two-electron four-center bonding interaction emerges from the overlap of the SOMO orbitals of the $[TCNE]^-$ and is not hypervalent.[36] Therefore, it cannot be present when the HOMO is doubly occupied. Hence, this cation-mediated $\pi^* - \pi^*$ CC bonding interaction complies with Pauling's definition of a chemical bond, that is, "…there is a chemical bond between two atoms or groups of atoms in the case that the forces acting between them are such as to lead to an aggregate with sufficient stability to make it convenient for the chemist to consider it as an independent molecular species."[26c] and exhibits all the physical properties expected from a classical CC covalent bond. Hence, this bonding interaction is unique; its two-electron bond resides over four chemically equivalent carbon atoms and involves the π^* orbitals of each fragment.

Experimental Section

All materials were prepared by routes previously described in the literature in a Vacuum Atmospheres Dri-Box under nitrogen. Infrared spectra were recorded for KBr pellets on a Bio-Rad FTS-40 FTIR spectrophotometer with ± 1 cm^{-1} resolution. Solid-state UV-visible spectra were recorded on a Hewlett–Packard 8452A diode array spectrophotometer, also as KBr pellets. A home-built cryostat based upon two 1 inch diameter quartz windows separated by a ~1 mm thick O-ring/Teflon spacer sample compartment was loaded in a Dri-Box and cooled to 77 K with liquid nitrogen was used for the solution UV/vis studies. For these studies $[Et_4N]_2[TCNE]_2$ was dissolved in dry MeTHF freshly distilled from sodium/benzophenone. Magnetic susceptibility studies were obtained on a Quantum Design MPMS 5T magnetometer as previously described.[37] The EPR spectra were recorded on an IBM/Bruker ER 200 D-SRC spectrometer. Ab initio UBLYP/6–31+G(2d,2p) computations were carried out by using the non-local B3LYP exchange and correlation DFT functional[38] and the 6–31+G(2d,2p) basis set,[39] with a determinant in which the orbitals are not restricted to be doubly occupied. All the computations were done using the Gaussian-98 suite of programs.[40] The critical point analysis was done by using the AIMPAC package.[41]

Acknowledgements

The authors gratefully acknowledge the support from the US National Science Foundation (Grant No. CHE 0110685), and the US DOE (Grant No. DE FG 03–93ER45504), as well as the extensive discussions with Jack Simons regarding the computational and experimental studies and Chuck Wight regarding the low-temperature electronic spectra studies and the

  0947-6539/02/0821-4906 $ 20.00+.50/0

loan of his cryostat. R.E.D.S. thanks the University of Utah Graduate School for a Graduate Research Fellowship. J.J.N and P.L. also thank the support of the CICYT (project PB98-1166-C02-02) and CIRIT (1999SGR-00046 and 2001-SGR-00044), and a grant of computer time provided by CESCA-CEPBA and the University of Barcelona. P.L. also thanks the Ministerio de Educación y Cultura for her doctoral fellowship grant.

[1] See, for example, *Handbook of Conducting Polymers* (Eds.: T. A. Skotheim, R. L. Elsenbaumer, J. R. Reynolds), 2nd ed., M. Dekker, New York, **1998**; *Handbook of Organic Conductive Molecules and Polymers* (Ed.: H. Nalwa), Wiley, Dekker, New York, **1997**; A. Graja, *Low-Dimensional Organic Conductors*, World Scientific, Singapore, **1992**; J. R. Ferraro, J. M. Williams, *Introduction to Synthetic Electrical Conductors*, Academic Press, Orlando, **1987**; S. Hünig, *J. Mater. Chem.* **1995**, *5*, 1469.

[2] See, for example, J. M. Williams, *Organic Superconductors (Including Fullerenes): Synthesis, Structure, Properties, and Theory*, Prentice Hall, Englewood Cliffs, NJ, **1992**; T. Ishiguro, K. Yamaji, G. Saito, *Organic Superconductors*, Springer, New York, **1998**.

[3] a) V. I. Ovcharenko, R. Z Sagdeev, *Russ. Chem. Rev.* **1999**, *68*, 345; b) J. S. Miller, A. J. Epstein, *Chem. Commun.* **1998**, 1319; c) W. Plass, *Chem. Unsere Zeit* **1998**, *32*, 323; d) J. S. Miller, A. J. Epstein *Chem. Eng. News* **1995**, *73*(40), 30; e) J. S. Miller, A. J. Epstein, *Angew. Chem.* **1994**, *106*, 399; *Angew. Chem. Int. Ed. Engl.* **1994**, *33*, 385; f) M. Kinoshita, *Jpn. J. Appl. Phys.* **1994**, *33*, 5718; g) A. Caneschi, D. Gatteschi, *Prog. Inorg. Chem.* **1991**, *37*, 331; h) A. L. Buchachenko, *Russ. Chem. Rev.* **1990**, *59*, 307; i) D. Gatteschi, *Adv. Mater.* **1994**, *6*, 635; j) O. Kahn, *Molecular Magnetism*, VCH, New York, NY, **1993**.

[4] J. S. Miller, D. A. Dixon, *Science* **1987**, *235*, 871.

[5] a) J. S. Miller, J. C. Calabrese, H. Rommelmann, S. Chittipeddi, A. J. Epstein, J. H. Zhang, W. M. Reiff, *J. Am. Chem. Soc.* **1987**, *109*, 769; b) J. S. Miller, D. T. Glatzhofer, D. M. O'Hare, W. M. Reiff, A. Chakraborty, A. J. Epstein, *Inorg. Chem.* **1989**, *28*, 2930; c) A. Zheludev, A. Grand, E. Ressouche, J. Schweizer, B. Morin, A. J. Epstein, D. A. Dixon, J. S. Miller, *J. Am. Chem. Soc.* **1994**, *116*, 7243; d) T. V. Baukova, O. G. Ellert, L. G. Kuz'mina, N. V. Dvortsova, D. A. Lemenovskii, A. Z. Rubezhov, *Mendeleev Commun.* **1991**, 22; e) S. Flandrois, K. Ludolf, H. J. Keller, D. Nöthe, S. R. Bodeson, Z. G. Soos, D. Wehe, *Mol. Cryst. Liq. Cryst.* **1983**, *95*, 149; f) J. S. Miller, D. A. Dixon, J. C. Calabrese, C. Vazquez, P. J. Krusic, M. D. Ward, E. Wasserman, R. L. Harlow, *J. Am. Chem. Soc.* **1990**, *112*, 381; g) S. Barlow, V. J. Murphy, J. S. O. Evans, D. O'Hare, *Organometallics* **1995**, *14*, 3461.

[6] J. Zhang, L. M. Liable-Sands, A. L. Rheingold, R. E. Del Sesto, D. C. Gordon, B. M. Burkhart, J. S. Miller, *Chem. Commun.* **1998**, 1385.

[7] a) M. M. Olmsted, G. Speier, L. Szabo, *J. Chem. Soc. Chem. Commun.* **1994**, 541; b) J. S. Miller, D. M. O'Hare, A. Charkraborty, A. J. Epstein, *J. Am. Chem. Soc.* **1989**, *111*, 7853; c) D. A. Lemervoskii, R. A. Stukan, B. N. Tarasevich, Tu. L. Slovokhotov, M. Yu. Antipin, A. E. Kalinin, Yu. T. Struchov, *Struct. Khim.* **1981**, *7*, 240; d) H. Bock, K. Ruppert, D. Fenske, H. Goesmann, *Z. Anorg. Allg. Chem.* **1991**, *595*, 275; e) J. S. Miller, D. T. Glatzhofer, C. Vazquez, R. S. McLean, J. C. Calabrese, W. J. Marshall, J. W. Raebiger, *Inorg. Chem.* **2001**, *40*, 2058; f) S. A. Clemente, A. Marzotto, *J. Mater. Chem.* **1996**, 941; g) M. T. Johnson, C. F. Campana, B. M. Foxman, W. Desmarais, M. J. Vela, J. S. Miller, *Chem. Eur. J.* **2000**, *6*, 1805; h) J. R. Fox, B. M. Foxman, D. Guerrer, J. S. Miller, A. H. Reis, Jr., *J. Mater. Chem.* **1996**, *6*, 1627; i) R. E. Del Sesto, R. E. Sommer, J. S. Miller, *CrystEngComm* **2001**, *3*, 47; j) H. Bock, C, Nather, K. Ruppert, *Z. Anorg. Allg. Chem.* **1992**, *614* 109; k) J. S. Miller, D. A. Dixon, J. C. Calabrese, C. Vazquez, P. J. Krusic, M. D. Ward, E. Wasserman, R. L. Harlow, *J. Am. Chem. Soc.* **1990**, *112*, 381; l) H. Bock, K. Ruppert, *Inorg. Chem.* **1992**, *31*, 5094; m) R. E. Del Sesto, M. Botoshansky, M. Kaftory, J. S. Miller, *CrystEngComm* **2002**, *4*, 106.

[8] J. J. Novoa, P. Lafuente, R. E. Del Sesto, J. S. Miller, *Angew. Chem.* **2001**, *113*, 2608; *Angew. Chem. Int. Ed.* **2001**, *40*, 2540.

[9] C. Vazquez, J. C. Calabrese, D. A. Dixon, J. S. Miller, *J. Org. Chem.* **1993**, *58*, 65.

[10] G. Kaupp, J. Boy, *Angew. Chem.* **1997**, *109*, 48; *Angew. Chem. Int. Ed.* **1997**, *36*, 48; F. Toda, *Eur. J. Org. Chem.* **2000**, 1377.

[11] W. D. Phillips, J. C. Powell, *J. Chem. Phys.* **1960**, *33*, 626; R. Chang, *J. Phys. Chem.* **1970**, *74*, 2029; D. B. Chesnut, W. D. Phillips, *J. Chem. Phys.* **1961**, *35*, 1002.

[12] M. Itoh, *Bull. Chem. Soc. Jap.* **1972**, *45*, 1947.

[13] S. Mikami, K-i. Sugiura, J. S. Miller, Y. Sakata, *Chem. Lett.* **1999**, 413; H. Zhao, R. A. Heinz, K. R. Dunbar, R. D. Rogers, *J. Am. Chem. Soc.* **1996**, *118*, 12844; R. H. Harms, H. J. Keller, D. Nöthe, M. Werner, D. Grundel, H. Sixl, Z. G. Soos, R. M. Metzger, *Mol. Cryst. Liq. Cryst.* **1981**, *65*, 179; S. K. Hoffman, P. J. Corvan, P. Singh, C. N. Sethuklekshmi, R. M. Metzer, W. E. Hatfield, *J. Am. Chem. Soc.* **1983**, *105*, 4608; V. Dong, H. Endres, H. J. Keller, W. Moroni, D. Nöthe, *Acta Crystallogr. Sect. B* **1977**, *33*, 2428.

[14] a) P. Becker, P. Coppens, R. K. Ross, *J. Am. Chem. Soc.* **1973**, *95*, 7604; b) R. G. Littel, D. Paultier, P. Coppens, *Acta Crystallogr. Sect. B* **1971**, *27*, 1493; U. Druck, H. Guth, *Z. Kristallogr.* **1982**, *161*, 103.

[15] D. A. Dixon, J. S. Miller, *J. Am. Chem. Soc.* **1987**, *109*, 3656.

[16] a) $[C_2H_4]^{\bullet-}$ UB3LYP/6–31+G(2d,2p) calculations; b) $[C_2F_4]^{\bullet-}$ UB3LYP/6–31+G(2d,2p) calculations.

[17] A. Szabo, N. S. Ostlund, *Modern Quantum Chemistry*, Academic Press, Macmillan, New York, **1982**, Chapters 3 and 4.

[18] R. D. Harcourt, *J. Phys. Chem.* **1991**, *95*, 6916.

[19] M. L. McKee, M. Bühl, O. P. Charkin, P. von R. Schleyer, *Inorg. Chem.* **1993**, *32*, 4549.

[20] a) M. Bremer, P. von R. Schleyer, K. Schötz, M. Kausch, M. Schinder, *Angew. Chem.* **1987**, *99*, 761; *Angew. Chem. Int. Ed.* **1987**, *26*, 761; b) G. K. S. Prakash, V. V. Krishnamurthy, R. Herges, R. Bau, G. Olah, W-D. Fessner, H. Prinzbach, *J. Am. Chem. Soc.* **1986**, *108*, 836; c) R. Herges, P. von R. Schleyer, M. Schinder, W.-D. Fessner, *J. Am. Chem. Soc.* **1991**, *113*, 3649.

[21] a) J. J. Novoa, M.-H. Whangbo, J. M. Williams, *J. Chem. Phys.* **1991**, *94*, 4835; b) J. J. Novoa, P. Lafuente, F. Mota, *Chem. Phys. Lett.* **1998**, *290*, 519.

[22] P. Hobza, R. Zahradnik, *Intermolecular Complexes*, Elsevier, Amsterdam, **1988**.

[23] R. F. Bader, *Atoms in Molecules*, Clarendon, Oxford, **1990**.

[24] J. Cioslowski, S. T. Mixon, *J. Am. Chem. Soc.* **1992**, *114*, 4382.

[25] C. A. Hunter, J. K. M. Sanders, *J. Am. Chem. Soc.* **1990**, *112*, 5525.

[26] L. Pauling, *The Nature of the Chemical Bond*, 3rd ed., Cornell University Press, Ithaca, NY, **1960**; a) p. 260; b) p. 122; c) p. 6.

[27] a) D. Braga, F. Grepioni, J. J. Novoa, *Chem. Commun.* **1998**, 1959; b) J. J. Novoa, I. Nobeli, F. Greppioni, D. Braga, *New. J. Chem.* **2000**, 5; c) J. J. Novoa, in *Implications of Molecular Materials Structure for New Technologies* (Eds.: J. A. K. Howard, F. H. Allen, G. P. Shields), Kluwer, Amsterdam, **1999**.

[28] D. Braga, F. Greppioni, F. Mota, J. J. Novoa, *Chem. Eur. J.*, **2002**, *8*, 1163; D. Braga, L. Maini, F. Grepioni, F. Mota, C. Rovira, J. J. Novoa, *Chem. Eur. J.*, **2000**, **6**, 4536.

[29] $\pm x$ is the standard deviation from the average.

[30] The red color of dimer is also evident in for $[Et_4N]_2[TCNE]_2$ dissolved in CH_2Cl_2 (mp = 178 K (−95 °C)) solution at 195 K (−78.5 °C; dry ice/Me_2CO bath) or at 178 K (−95 °C; PhMe/N_2(l) slush), and the red color is more intense at lower temperatures. In contrast, the red color of dimer does not appear when $[n\text{Bu}_4\text{N}][TCNE]$, which does not form a dimer in the solid state,[5c] is dissolved in MeTHF and is cooled to 77 K.

[31] The orbital energy between occupied and empty orbitals is an arbitrary value at the Hartree–Fock level because the orbital energy of the empty orbitals is arbitrary. Therefore, it is meaningless to look at the orbital energy to obtain this value.

[32] J. B. Foresman, M. Head-Gordon, J. A. Pople, M. J. Frisch, *J. Phys. Chem.* **1992**, *96*, 135.

[33] Plus two additional weak peaks (~10% as intense as the stronger peaks) at ~2200 cm^{-1}.

[34] Similar results were noted for π-$[TCNQ]_2^{2-}$: M. J. Rice, N. O. Lipari, S. Strassler, *Phys. Rev. Lett.* **1977**, *39*, 1359.

[35] It should be noted that cation-mediated π-$[TCNE]_2^{2-}$ dimers need not form, for example, $[(n\text{Bu}_4\text{N}][TCNE]$ possesses isolated $[TCNE]^{\bullet-}$ radical ions.[5c]

[36] It should be noted that in addition to the short π–CC bonding interactions, longer $[TCNE]^- \cdots [TCNE]^-$ interactions are frequently present, but at these long distances (>3.5 Å) the bonding properties

disappear, due to the exponential of the orbital overlaps responsible for Δ.

[37] E. J. Brandon, D. K. Rittenberg, A. M. Arif, J. S. Miller, *Inorg. Chem.* **1998**, *37*, 3376.

[38] The B3LYP is a combination of the nonlocal three parameters exchange functional (A. D. Becke, *J. Chem. Phys.* **1993**, *98*, 5648) and nonlocal LYP correlation functional (C. Lee, W. Yang, R. G. Parr, *Phys. Rev. B* **1998**, *37*, 785).

[39] a) R. Ditchfield, W. J. Hehre, J. A. Pople, *J. Chem. Phys.* **1971**, *54*, 724; b) T. Clark, J. Chandrasekhar, G. W. Spitznagel, P. von R. Schleyer, *J. Comp. Chem*. **1983**, *4*, 294.

[40] Gaussian 98, Revision A.7, M. J. Frisch, G. W. Trucks, H. B. Schlegel, G. E. Scuseria, M. A. Robb, J. R. Cheeseman, V. G. Zakrzewski, J. A. Montgomery, Jr., R. E. Stratmann, J. C. Burant, S. Dapprich, J. M. Millam, A. D. Daniels, K. N. Kudin, M. C. Strain, O. Farkas, J. Tomasi, V. Barone, M. Cossi, R. Cammi, B. Mennucci, C. Pomelli, C. Adamo, S. Clifford, J. Ochterski, G. A. Petersson, P. Y. Ayala, Q. Cui, K. Morokuma, D. K. Malick, A. D. Rabuck, K. Raghavachari, J. B. Foresman, J. Cioslowski, J. V. Ortiz, A. G. Baboul, B. B. Stefanov, G. Liu, A. Liashenko, P. Piskorz, I. Komaromi, R. Gomperts, R. L. Martin, D. J. Fox, T. Keith, M. A. Al-Laham, C. Y. Peng, A. Nanayakkara, C. Gonzalez, M. Challacombe, P. M. W. Gill, B. Johnson, W. Chen, M. W. Wong, J. L. Andres, C. Gonzalez, M. Head-Gordon, E. S. Replogle, and J. A. Pople, Gaussian, Inc., Pittsburgh PA, 1998.

[41] F. Biegle-Kröning, R. F. W. Bader, W.-H. Tang, *J. Comput. Chem*. **1982**, *3*, 317.

Received: April 16, 2002 [F4019]

  0947-6539/02/0821-4908 $ 20.00+.50/0